DECARBURIZATION OF AN IRON 0.8% CARBON ALLOY IN THE PRESENCE OF A WUSTITE SCALE

DECARBURIZATION OF AN IRON 0.8% CARBON ALLOY IN THE PRESENCE OF A WUSTITE SCALE

By

ANDREW STEWART REEVES, B.Sc.

A Thesis

Submitted to the Faculty of Graduate Studies

in Partial Fulfilment of the Requirements

for the Degree

Master of Science

McMaster University

September 1967

Master of Science (Metallurgy) 1967 McMaster University
Hamilton, Ontario

TITLE: Decarburization of an Iron-0.8% Carbon Alloy in the Presence of a Wustite Scale

AUTHOR: Andrew Stewart Reeves, B.Sc. (Hon.)
(Dalhousie University)

SUPERVISOR: Professor W. W. Smeltzer

NUMBER OF PAGES: viii, 81

ABSTRACT: The kinetics of the oxidation and decarburization of an iron-0.8% carbon alloy in carbon dioxide at 950°C have been studied. Both processes are controlled by surface reactions. Decarburization through the wustite scale has been studied by allowing oxide reduction by carbon to proceed under vacuum and in argon atmosphere. Oxide reduction is influenced both by surface reaction steps and by carbon diffusion in the metal. Transport of the gaseous reaction products through the scale is accomplished primarily by porosity in the oxide, with occasional evidence of mechanical failure of wustite. The effectiveness of the pores as a means of transport of carbon gases is dependent on the wustite scale thickness and a critical concentration of carbon at the metal-oxide interface.

Acknowledgements

The author wishes to express sincere gratitude to all individuals and organizations who have helped in this investigation, particularly the following: Dr. W. W. Smeltzer, the research supervisor, for his encouragement, guidance, criticism and supervision at all stages of the investigation; Dr. G. R. Purdy, who supplied the alloys used in this study; Dr. L. A. Morris, who designed and built the apparatus; Mr. M. van Oosten, for assistance with chemical analyses, photography and specimen preparation; The American Iron and Steel Institute, for a research grant to Dr. Smeltzer; The Defence Research Board of Canada, for provision of a leave of absence from employment, and for financial assistance in the form of a Defence Research Board Scholarship.

TABLE OF CONTENTS

LIST OF ILLUSTRATIONS

CHAPTER I

INTRODUCTION

In the iron and steel industry, quality control of finished products is of major importance because of rigorous demands made on steels by the consumer. Steels generally must be of uniform structure and composition and exhibit sufficient strength for different design specifications. Extensive surface oxidation is usually undesirable because an excessive amount of metal is wasted and selective oxidation of alloying elements leads to steels of inferior mechanical properties. Decarburization, the selective removal of carbon from the surface of the metal, results in a layer of low-carbon metal at the surface. From the point of view of mechanical properties, this situation is undesirable because the decarburized layer is softer than the rest of the metal and the fatique resistance of a steel is impaired.

Decarburization occurs by a process involving diffusion of carbon in the metal to the surface, chemical reaction with the surrounding media, and loss of carbon as either gaseous carbon monoxide or carbon dioxide.

Since it is not known precisely how these processes are affected by the presence of an oxide layer, the purpose of this investigation was to attempt to discover how carbon penetrates through a superficial wustite scale.

Oxidation behaviour of steels, consisting of iron, carbon and several other elements is extremely complex. In order to simplify the system, the study has been restricted to binary alloys of iron and carbon. Even this system exhibits complexities. One of the reaction products is a gas. Also, three oxides of iron can be formed in the scale depending on oxidation conditions. However, it is possible by working in atmospheres of low oxygen potential to produce only one oxide. This was done in this investigation, and all oxidation experiments were carried out in carbon dioxide atmospheres under conditions where only one oxide of iron was formed, i.e., wustite. Also it was hoped to simplify the theoretical considerations by examining reaction kinetics in two stages, consisting of simultaneous oxidation of iron and carbon until a layer of wustite formed on the metal surface, then allowing decarburization to proceed without further wustite formation.

This work is a continuation of the research initiated by G. J. Billings during completion of his M.Sc.

degree research on the oxidation-decarburization kinetics of iron-carbon alloys in carbon dioxide-carbon monoxide atmospheres.

CHAPTER II

LITERATURE REVIEW

2.1 Introduction

In this section, the literature relevant to the problem of decarburization of steel through a superficial oxide scale will be briefly discussed. For a more comprehensive view of the broader field of metal oxidation, the reader is urged to consult one of the numerous textbooks and review articles which have appeared on this subject, among which may be mentioned works by Kubaschewski and Hopkins[1], Hauffe[2], and Kofstad[3].

2.2 Oxidation of Metals

With the exception of gold, all metals and alloys form one or more stable oxides upon exposure to normal atmospheric conditions. The type of oxide formed and the rate at which it is formed vary widely, depending on the metal under consideration, and on external factors such as temperature, pressure, and type of oxidizing atmosphere.

2.2.1 Properties of Oxides

Most oxides formed on the surface of a metal are not stoichiometric, having either an excess of oxygen or a deficiency of oxygen. They are semi-conductors and have conductivities several orders of magnitude lower than that of a metal. The temperature coefficient of conductivity is positive, in contrast to metallic conductors. The conductivity is, therefore, primarily electronic, and is derived from movement of either electrons or electron holes. Where conductivity occurs by transport of electrons, the oxides are characterized by either excess ions present in interstitial positions in the oxide lattice, such as BeO, or by anion vacancies in lattice positions, such as ZrO_2. These oxides are deficient in oxygen and are n-type semi-conductors. Similarly, where conductivity occurs by motion of electron holes, the oxides are characterized by cation vacancies in lattice positions, such as CoO and FeO. These oxides have an excess of oxygen and are p-type semi-conductors. Diffusion rates in the scale are dependent on defect concentration, and tend to decrease as the stoichiometric composition is approached, since in this limiting case little or no concentration gradient can exist. This may be offset by solubility of small amounts of oxygen or excess metal. If diffusion of cations through the oxide layer is predominant, growth of the oxide occurs at the oxide-gas interface, while anion diffusion leads to growth at the metal-oxide interface.

2.2.2 Rate Laws

Oxidation rates are found experimentally by determining the oxide thickness as a function of time. Optical, gravimetric, volumetric, and electrical methods have been used. Perhaps the most common method of measurement is to record oxygen uptake gravimetrically as a function of time. Oxygen uptake per unit area ($\frac{\Delta m}{A}$) is directly proportional to oxide thickness (Equation 1) if it can be assumed that the density is constant throughout the oxide layer.

$$\frac{\Delta m}{A} = \frac{\text{Mol. wt. of oxygen}}{\text{Mol. wt. of oxide}} \cdot \rho \cdot x \qquad (1)$$

where x is the oxide thickness and ρ is the density.

The simplest possible rate law is a linear relationship, i.e.,

$$\Delta m/A = k_{\ell} t \qquad (2)$$

This type of behaviour is associated with growth of porous films where there is direct contact between metal and gas, such as the alkali metals. It is also observed in growth of more compact scales such as wustite, in cases where the rate-controlling step is a chemical reaction at the metal-oxide interface.

The most common type of oxidation behaviour, and also the best-understood from a theoretical point of view is the parabolic relationship. In this case the oxidation rate is inversely proportional to the film thickness, i.e.,

$$\frac{dx}{dt} = \frac{k}{x} \qquad (3)$$

Integration of equation 3 and substitution in equation 1 yields the parabolic relationship

$$(\Delta m/A)^2 = k_p t + C \qquad (4)$$

If this law applies from time zero, the constant of integration is zero.

The rate-controlling process is diffusion of either cations or anions across a relatively compact oxide layer. Detailed theoretical treatment of the oxide growth process, in terms of electrical conductivity and transport numbers of ions and electrons, has been carried out by Wagner[4,5]. Experimental evidence in support of Wagner's theory has been obtained for several metals, including iron[6].

Other rate laws which have been observed experimentally are the cubic, logarithmic and inverse logarithmic, shown in equations 5, 6 and 7 respectively:

$$\text{Cubic} \qquad (\Delta m/A)^3 = k_c t \tag{5}$$

$$\text{Logarithmic} \qquad \Delta m/A = k_e \log(at+t_o) \tag{6}$$

$$\text{Inverse logarithmic} \qquad \frac{1}{\Delta m/A} = A - k_i \log t \tag{7}$$

These relationships are most applicable in describing formation of very thin films (<100 Å), where a large electric field can exist, and oxidation rates are determined by movement of charged particles (electrons and ions) in the thin films. Development of this theory is due largely to Cabrera and Mott[7] and Hauffe and Ilschner[8].

In most cases, the temperature effect of the rate laws previously described can be expressed by an Arrhenius relationship

$$k = k_o \, e^{-Q/RT} \tag{8}$$

and the activation energy of the rate-controlling process can be estimated.

2.2.3 Alloy Oxidation

Alloy oxidation is extremely complex. In addition to the structural features associated with oxide growth according to one or more of the common rate laws, other problems which may be encountered include (1) formation of more than one oxide, either in distinct layers or as one oxide dispersed in another; (2) formation of spinels, or double oxides of variable composition; (3) selective oxidation; (4) internal oxidation;

(5) differences in diffusion rates in the metal substrate;
(6) affinity of component metals for each other and for oxygen;
(7) mutual solubilities in the oxidation layers. By consideration of such topics as the effect on defect structure of an oxide by adding a metal of different valence, and which metals form highly protective oxides, the oxidation behaviour of most binary alloys can be described qualitatively, but there are usually too many interrelated variables for quantitative theoretical analysis. For multicomponent commercial alloys, the most useful information is obtained by service tests.

2.3 Oxidation of Iron

In view of the fact that this investigation is concerned with iron-carbon alloys, of which only iron forms solid oxides, the oxidation behaviour of iron should be discussed, particularly in atmospheres of low oxygen potential.

The iron-oxygen phase diagram has been studied in detail by several investigators. Probably the most accurate work is that of Darken and Gurry[9]. It may be seen that three stable oxides of iron can be formed, wustite (FeO), magnetite (Fe_3O_4) and hematite (Fe_2O_3). Below 570°C, wustite is not stable in bulk, although it is sometimes observed in the form of a film adjacent to the metal surface at temperatures as low as 400°C. The phase field of wustite extends from about 51 to 54 atomic percent oxygen which does not include the stoichiometric composition. This shows that the concentration of lattice

defects must be unusually high in this oxide, and the large defect concentration explains why diffusion rates in wustite are higher than in most oxides. Magnetite also exists with an excess of oxygen, but the deviation from stoichiometry, and hence the defect concentration, is considerably less than in wustite. Hematite is a metal-excess oxide, with a very small phase field. Growth of wustite occurs by cation diffusion, while anion diffusion predominates in hematite, and both cations and anions diffuse in magnetite.[10,11]

When more than one oxide can be formed under given oxidizing conditions, the oxide richest in metal is formed adjacent to the metal and that richest in oxygen is formed next to the gas phase, thus establishing concentration gradients of metal and oxide across the scale. Thus on iron at temperatures above 570°C, a layered structure of $Fe/FeO/Fe_3O_4/Fe_2O_3/O_2$ would be expected. This has been frequently observed. Paidassi[12] has shown by careful metallography that the ratio of thicknesses of $FeO:Fe_3O_4:Fe_2O_3$ remains almost constant at 100:5:1 at temperatures above 700°C. The kinetics of oxidation of iron are usually described by a logarithmic rate equation at temperatures below 200°C[13], and by a parabolic relationship at higher temperatures[11]. The Wagner mechanism for diffusion of matter through the various oxides has been shown to be applicable[6].

The above statements are applicable in atmospheres where P_{O_2} exceeds the dissociation pressure of all of the oxides of iron. In gas mixtures such as H_2O/H_2 and CO_2/CO, the following equilibria must also be considered:

$$H_2O \rightleftharpoons H_2 + \frac{1}{2} O_2 \qquad (9)$$

$$CO_2 \rightleftharpoons CO + \frac{1}{2} O_2 \qquad (10)$$

from which it may be shown that

$$P_{O_2} = \left(K \cdot \frac{P_{CO_2}}{P_{CO}} \right)^2 \qquad (11)$$

where K is the equilibrium constant for equation 10. It is found that for these gas mixtures the dissociation pressures of magnetite and hematite are not exceeded, and the only oxide formed is wustite.

Hauffe and Pfeiffer[14] observed linear oxidation rates with iron in CO_2-CO atmospheres at 900° - 1000°C, indicating that the rate-controlling step was not diffusion through the oxide, but instead a phase-boundary reaction. However the oxidation rate was found to be a function of the CO_2/CO ratio. If the interface reaction was rate determining, the oxidation rate should be independent of pressure. This led the authors to suggest that the rate controlling reaction is chemisorption of the oxygen produced at the surface by decomposition of CO_2 (equation 12) which was followed by

formation of a new wustite lattice site (equation 13)

$$CO_2 \longrightarrow O^-_{ads.} + CO + \oplus \qquad (12)$$

$$O^-_{ads.} \longrightarrow FeO + Fe^{++}\square + \oplus \qquad (13)$$

where $\oplus$ denotes a positive hole, and $Fe^{++}\square$ is an iron cation vacancy.

Smeltzer[15] found that oxidation kinetics of iron in CO_2 in the temperature range 600° - $1100^{\circ}C$ were linear, transforming to parabolic at long times. The following reaction mechanism was proposed:

$$CO_2 \longrightarrow O^{=}_{ads.} + 2\,\oplus_{(o)} + CO \qquad (14)$$

$$O^{=}_{ads.} \longrightarrow FeO + Fe^{++}\square_{(o)} \qquad (15)$$

$$Fe^{++}\square_{(o)} + 2\,\oplus_{(o)} \rightleftharpoons Fe^{++}\square_{(i)} + 2\,\oplus_{(i)} \qquad (16)$$

$$Fe + Fe^{++}\square_{(i)} + 2\,\oplus_{(i)} \rightleftharpoons Nil \qquad (17)$$

$$O^{=}_{ads.} + 2\,\oplus_{(o)} \longrightarrow \tfrac{1}{2}\,O_2 \qquad (18)$$

Subscripts (o) and (i) refer to oxide-gas interface and metal-oxide interface respectively. "Nil" refers to annulment of lattice defects by solution of iron into the oxide.

If diffusion of iron vacancies across the oxide scale (equation 16) is the rate-controlling step, then a parabolic oxidation rate would be observed. Since linear kinetics are observed in the early stages of the reaction, the rate-determining step must be the chemisorption of oxygen (equation 14) or the absorption of chemisorbed oxygen into the wustite lattice (equation 15). By assuming that the surface coverage of adsorbed oxygen remained constant, and that lattice defects in the oxide were in equilibrium with the metal, Smeltzer derived an expression for the dependence of the linear rate constant, k_ℓ, on CO_2 partial pressure

$$k_\ell = \text{constant } (P_{CO_2} - P_{CO_2}^*) \qquad (19)$$

where $P_{CO_2}^*$ is the partial pressure of CO_2 over wustite equilibrated with iron.

Nearly simultaneously, Pettit, Yinger and Wagner[16] derived a similar expression, assuming that chemisorption (equation 14) was the rate-controlling step. They also found that k_ℓ is directly proportional to P, the sum of partial pressures of CO_2 and CO. Linear oxidation rates were observed up to an oxide thickness of 10^{-2} cm., and parabolic rates for thicker scales. In a later paper, Pettit and Wagner[17] presented a theory describing the transition from linear to parabolic kinetics, which agreed well with their experimental observations. In more recent publications,

Grabke[18], and Morris and Smeltzer[19] have demonstrated that a detailed balance of the surface reaction steps for dissociation of CO_2 and incorporation of chemisorbed oxygen into wustite lead to the expression

$$k_\ell = k(1+K)(P_{CO_2} - P_{CO_2}^*) \qquad (20)$$

where K is the equilibrium constant for the equilibration of iron with wustite, and k is the rate constant for dissociation of CO_2 at the wustite surface.

2.4 Principles of Oxidation Involving the System Fe-C-O

2.4.1 Chemisorption

Chemisorption designates an adsorption through chemical forces, i.e., through complete transition of electrons and formation of polar bonds or through sharing of electrons and formation of covalent bonds. A distinguishing feature of chemisorption is an activation energy of the same order of magnitude as that of a chemical reaction, in contrast to physical adsorption, where the heats of adsorption and bond energies are much lower. Most gases are chemisorbed by transition metals much better than by other metals. This is believed to be associated with the presence of unoccupied d-orbitals in the transition metals.

2.4.2 Equilibrium in the System Fe-C-O

Smith[20] has studied the equilibrium of iron-carbon alloys in CO - CO_2 atmospheres, where wustite formation could not occur. In this case, the reaction under consideration is

$$C(\text{dissolved in } \gamma\text{-Fe}) + CO_2 \rightleftharpoons 2CO \qquad (21)$$

By equilibrating iron-carbon alloys in a known atmosphere of CO_2 - CO and analyzing for alloy carbon content, Smith determined the activity of carbon in austenite relative to graphite, which he considered as the standard state. These measurements enabled the carburization-decarburization behaviour of steels in the austenitic range to be determined, provided the CO_2/CO ratio, temperature and alloy composition are known. Similar information can be obtained in the ferritic range by using CH_4 - H_2 atmospheres.

2.4.3 Oxidation of Metal and Carbon in Binary Metal-Carbon Alloys

Webb, Norton and Wagner[21] have examined the oxidation behaviour of binary alloys of Ni-C, Mn-C, Ti-C and W-C. Three possible reaction sequences were suggested. These are (1) diffusion of carbon to the metal-oxide interface where it reacts with scale, (2) rupture of the scale caused by the buildup of pressure of carbon oxides, (3) diffusion of carbon through the scale without rupture of scale. The latter mechanism seemed to explain the rapid oxidation of C

in Ni-2.3%C, without a corresponding large increase in rate of NiO formation. The same mechanism is a possibility for Fe-C oxidation, since both NiO and FeO are metal-deficit oxides, although the defect concentration in wustite is much higher.

2.5 Decarburization of Steel

The selective removal of carbon from the surface of a steel is termed decarburization. As mentioned in the introduction, its effect on mechanical properties of the material is usually undesirable. Controlled atmospheres are employed wherever possible in heat treating practice to avoid decarburization. The work of Pennington[22] showed the formation of large columnar grains of ferrite near the surface of the metal at temperatures between the eutectoid and the α-γ transformation of pure iron. Columnar formation of ferrite was not observed at temperatures entirely in the austenitic range, although extensive decarburization occurred. Decarburization readily occurs because diffusion rates of carbon in iron are relatively high at elevated temperatures.

2.5.1 Diffusion in Metals

The motion of atoms through the lattice sites in a metal can usually be described by applying appropriate boundary conditions to Fick's Laws:

$$J = - D \frac{\partial C}{\partial x} \tag{22}$$

and

$$\frac{\partial C}{\partial t} = D \frac{\partial^2 C}{\partial x^2} \tag{23}$$

where J is the flux of material across a given plane at right angles to the diffusion, D is the diffusion coefficient, and $\frac{\partial C}{\partial x}$ is the concentration gradient.

The solution of equation 23 for the decarburization of a steel sheet is of the form

$$C - C_s = (C_o - C_s) \text{ erf } \frac{x}{2\sqrt{Dt}} \tag{24}$$

where C is the concentration of carbon at distance x from the surface, C_s is the surface concentration, and C_o is the bulk alloy concentration. This simplified solution is based on the assumption of a constant diffusion coefficient D, which is only approximately valid. In the iron-carbon system, D depends on composition. For a fixed carbon content, the diffusion coefficient may be expressed by the Arrhenius temperature relationship

$$D = D_o e^{-Q/RT} \tag{25}$$

2.5.2 Surface Reactions

Doehlmann[23] oxidized Ni, Co, Fe-C alloy foils in $CO-CO_2$ atmospheres over the temperature range 920° - 970°C. For his experimental conditions, diffusion processes in the metal or gas phase could not be rate-determining. He suggested a reaction mechanism in which the surface of the foil is

divided into active and inactive sites. Two parallel reactions occur via these sites. The first reaction sequence is

$$CO_2 \rightleftharpoons CO + O_{ads.} \text{ (inactive)} \tag{26}$$

$$O_{ads.}\text{(inactive)} \underset{\text{diffusion}}{\overset{\text{surface}}{\rightleftharpoons}} O_{ads.}\text{(active)} \tag{27}$$

$$C + O_{ads.}\text{ (active)} \rightleftharpoons CO \tag{28}$$

The rate-determining step is the surface diffusion of oxygen from inactive to active sites, reaction 27. The second reaction sequence is

$$CO_2 \rightleftharpoons O_{ads.}\text{ (active)} + CO \tag{29}$$

$$C_{(\gamma\text{-Fe})} + O_{ads.}\text{ (active)} \rightleftharpoons CO \tag{30}$$

where reaction 29 is rate-determining. The final expression for decarburization rate contained two corresponding terms:

$$-\frac{dc}{dt} = \left(k_1 P_{CO_2} + k_2 \frac{P_{CO_2}}{P_{CO}}\right)\left(1 - \frac{[C^*]}{[C]}\right) \tag{31}$$

where k_1 and k_2 are defined by equations 27 and 29 respectively, $[C^*]$ is the equilibrium concentration of carbon in the alloy for fixed P_{CO_2}/P_{CO} ratio and $[C]$ is the concentration of carbon in the alloy at any time.

Grabke[24], using radioactive C^{14} as a tracer, has followed the kinetics of oxygen exchange between CO_2 and CO over iron foil as a catalyst. Like Doehlmann, he proposed the reaction sequence of equations 29 and 30, with equation 29 being rate-determining. Using these assumptions, he derived the expression

$$-\frac{\dot{n}_C}{A} = k_2 P_{CO_2}\left(1 - \frac{[C^*]}{[C]}\right) \tag{32}$$

where $\dot{n}_C$ is the decarburization rate, A is the area of the specimen, $[C^*]$ is the equilibrium concentration of carbon in the austenite, $[C]$ is the concentration of carbon at any time, and k_2 is the rate constant of equation 29. In integrated form, this equation describes the change in carbon content as a function of time

$$-([C] - [C_o]) - [C^*] \ell n \left(\frac{[C^*] - [C]}{[C^*] - [C_o]}\right) = \frac{2k_2 P_{CO_2} t}{\delta} \tag{33}$$

where δ is the foil thickness, and $[C_o]$ is the initial concentration of carbon in iron. $[C_o]$ and $[C^*]$ can be found from the activity measurements of Smith[20].

Billings[25], using Eyring's[26] theory of absolute reaction rates, has applied this model to the initial stages of the kinetics of simultaneous oxidation and decarburization of iron-carbon alloys in CO_2 - CO atmospheres.

2.5.3 Effect of Unbroken Oxide Layer

The work of Engell and co-workers[27,28,29] indicated that specimens oxidized in air and in CO_2 - CO mixtures decarburized without rupture of scale taking place. This can be explained in one of two ways: (1) diffusion of carbon through the scale or (2) reaction at the metal-oxide interface of carbon with the oxide (equations 34 and 35)

$$C + FeO \longrightarrow Fe + CO \qquad (34)$$

$$CO + FeO \longrightarrow Fe + CO_2 \qquad (35)$$

followed by passage of the gaseous carbon oxides through pores in the scale.

Langer and Trenkler[30] oxidized pure iron and iron-carbon alloys in various atmospheres over the temperature range 920° - 1000°C. Their results showed a dependence of decarburization rate on Po_2. They concluded that there was a direct reaction between carbon and the gaseous phase, and that carbon diffused through the scale and burned at the oxide-gas interface to form CO or CO_2. The rate-controlling partial reaction was the dissociation of oxygen. The oxygen was preferentially consumed by the carbon, which hindered FeO formation, and reduced the scaling rate.

Since it has been established[31,32] that the solubility of carbon in wustite, and hence the possible carbon concentration gradient across the oxide layer, is very small, diffusion of carbon through the scale seems unlikely. Bohnenkamp and

Engell[29] proposed that pores are present in the scales on Fe-C alloys which allow for effusion of the carbon oxides, but not for effective transport of oxygen from the gas phase to the metal surface. Their findings were consistent with the assumption that pore formation required a critical amount of carbon in the alloy at the metal-oxide interface. It was also assumed that pores in the scale formed in the presence of carbon were closed during the progress of scaling until a steady state was attained with very narrow pores in the wustite scale.

The higher rate of carbon oxidation in an alloy of Fe-0.8%C at 850°C in the presence of oxide scale, compared with unscaled samples, showed that a direct reaction between carbon and the metal oxide according to equation 34 also occurred. In previous work[27], Engell summarized his results as follows for Fe-1.0%C at 1050°C as follows: For short oxidation times, decarburization is dependent on diffusion of carbon in the metal, and for longer times the transport of carbon through the scale layer is rate-determining.

2.5.4 Effect of Ruptured Oxide Layer

The possibility of scale rupture allowing passage of carbon oxides through the scale, has been discussed by Sachs and Brown[33], as well as by Webb, Norton and Wagner[21]. If carbon reacts with the oxide, the equilibrium pressure of CO or CO_2 formed by reactions 34 and 35 can be estimated from

thermodynamic data[34,35]. For example, at 900°C, austenite containing 1%C would be in equilibrium with FeO at a CO pressure of 15 atm. and a CO_2 pressure of 8 atm. At 1000°C the corresponding figures would be 30 atm. and 15 atm. respectively. Measurements by Engell and Peters[36,37] indicate that the adhesive strength of FeO to the metal is about 100 kg/cm^2 (1 atm $\simeq$ 1 kg/cm^2)[38] on pure iron, and considerably less, e.g., 30 kg/cm^2 on mild steel. Thus the equilibrium pressure of CO according to reaction 34 and the cohesion strength of the scale are of the same order of magnitude. In the case of a small blocked pore in a thick scale, the circumferential stress is equal to the internal pressure, so that the equilibrium pressure of carbon oxides may be high enough to rupture the scale. If this happens, decarburization can proceed, whereas if the scale withstands the internal pressure, decarburization will occur only if the gaseous products can escape through open pores or other macroscopic defects in the scale. If the scale is ruptured, this should be reflected by sudden increases in the oxidation rates of both carbon and iron, insofar as the oxidizing atmosphere has free access to the metal surface.

CHAPTER III

EXPERIMENTAL METHODS

3.1 Apparatus

3.1.1 General Description

For most experiments, the only gas used was bone dry CO_2, supplied by Matheson of Canada Ltd. The purity of this gas, as stated by the manufacturer, was better than 99.95%. In a few experiments, a mixture of CO_2 and argon was used. The argon was supplied by Canadian Liquid Air Ltd., and the impurity content was not known. The CO_2 was passed through a purifying train consisting of silica gel and reduced copper oxide at 400°C. The argon was purified by passing it through magnesium perchlorate and ascarite. After purification the gases passed through capillary flowmeters containing dibutyl phthalate. Flow rates of gas in the furnace tube in all experiments were sufficiently rapid to avoid the undesirable effects of thermal segregation as described by Darken and Gurry[39]. For CO_2, the flowmeter calibration of Billings[25] was

used, and for argon a new calibration curve was prepared by measuring rate of displacement of water in a graduated cylinder. This curve is shown in Figure 3-1.

Photographs of the oxidation apparatus have been presented in the theses of Morris [40] and Billings [25]. Accordingly only a brief description of the salient features of this apparatus is presented, together with a schematic diagram of the oxidation assembly (Fig. 3-2).

The gases were passed through a one-liter mixing bulb filled with glass wool and admitted to the bottom of the furnace. The gas then flowed through an outlet at the top of the furnace, vented outside the building. Pressure fluctuations were overcome by using a capillary and an oil damping pot between the mixing bulb and the furnace. The entire essembly could be evacuated to a residual pressure of 10^{-5} Torr by means of a one-inch oil diffusion pump backed by a two-stage mechanical pump. Pressure inside the reaction chamber was measured by means of an open-end mercury manometer or by a Balzers ion gauge. The only modification to the apparatus from the original design of Morris [40] was that the vacuum pumps were connected to the gas inlet tube to the furnace, instead of at the top of the furnace. This did not affect the performance of the vacuum system, but did reduce the strain in the glassware at the top of the furnace.

Figure 3-1 Calibration of Argon Flowmeter

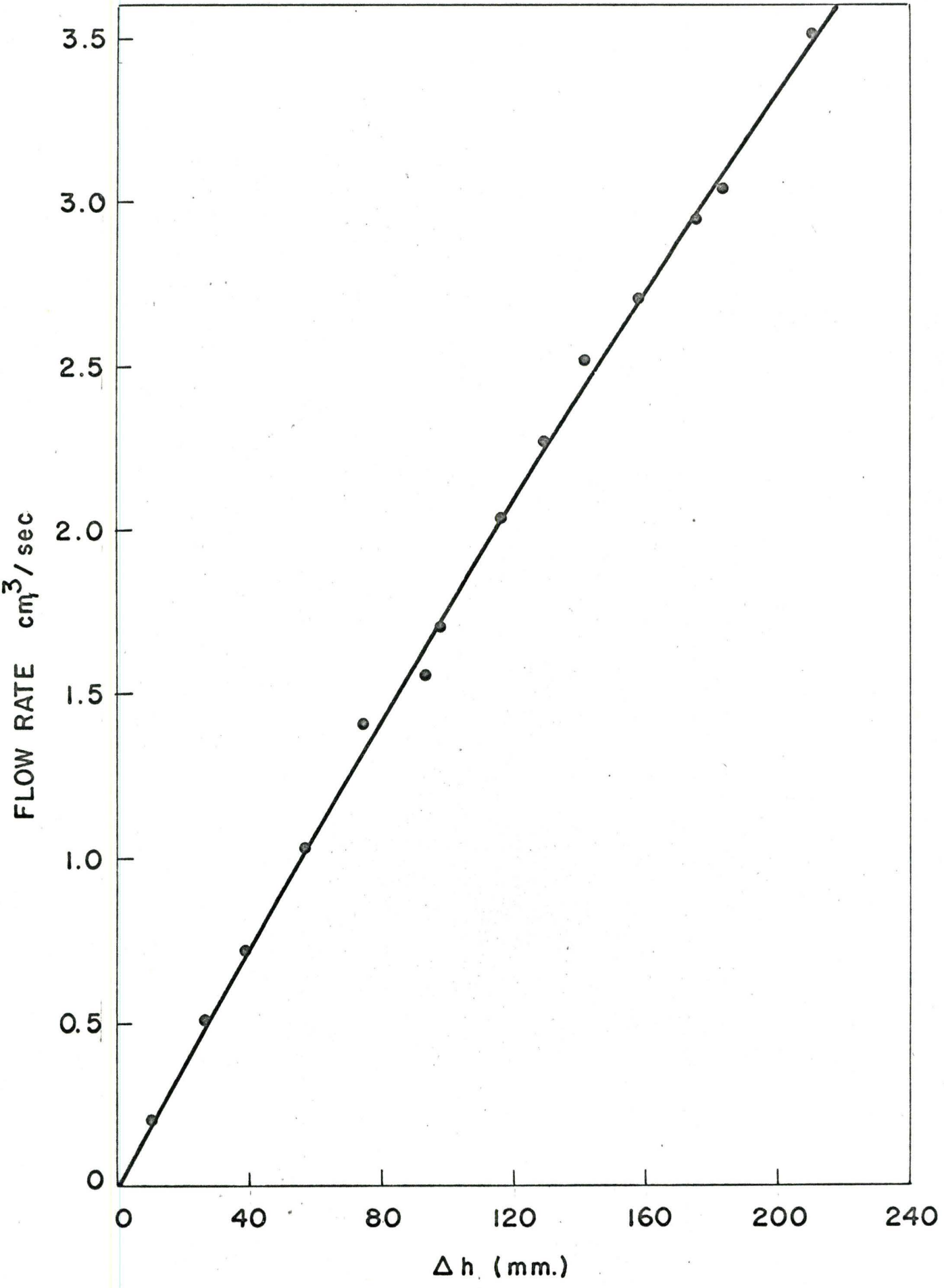

Figure 3-2 Schematic Diagram of Oxidation Assembly

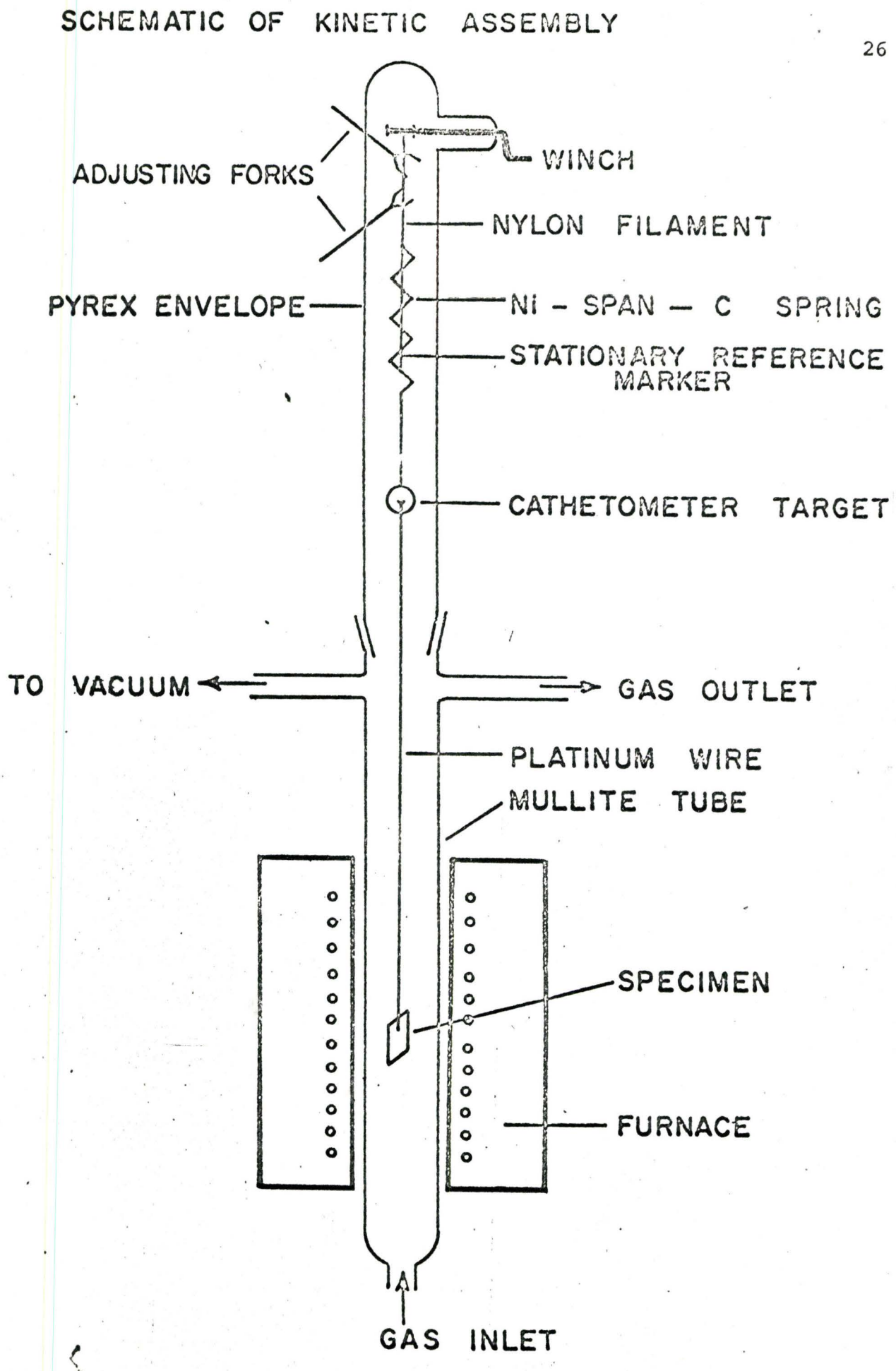

For experiments where alloy specimens were exposed to the flowing reactant gas at reduced pressure, a second mechanical pump was added at the furnace outlet. A reduced pressure could be maintained inside the reaction chamber by proper manipulation of the stopcocks at the inlet and outlet of the furnace.

3.1.2 Furnace

The furnace assembly consisted of a 20 inch Kanthal element imbedded in insulation surrounding a mullite reaction tube, $1\frac{1}{4}$ inch diameter and 30 inches in length. Power was supplied to the heating element from a 220 V line through a 2500 V.A. transformer. The temperature was controlled to $\pm 2^{\circ}C$ by a Phillips controller and a chromel-alumel thermocouple connected to a mercury relay in the supply circuit. The control thermocouple was placed between the mullite tube and the Kanthal windings at the center of the hot zone and a reference thermocouple was placed at the same level. Pyrex glass was sealed directly to the mullite tube in order to make a tight connection to the oxidation assembly.

3.1.3 Oxidation Assembly

In the oxidation assembly, the specimen was suspended on a hook of 10 mil platinum wire which was joined by a length of 5 mil platinum wire to a Ni-Span-C spring. The spring was suspended from a glass winch by a nylon thread

and the end of this rod served as a reference point. A marker was attached to the spring in order to measure the extension of the spring with a vernier cathetometer.

Ni-Span-C is an age hardenable alloy of nickel, iron, titanium and chromium. It has a high elastic limit in the hardened condition. Heat treatment was selected by Morris[40] to give a zero temperature coefficient of expansion over the temperature range 50^{o}-150^{o}F. The spring was calibrated in the operating range by measuring the extension produced by various accurately weighed samples. The calibration curve is shown in Figure 3-3, and yields a force constant of 30.5 mg/cm. The designer's intention was to measure the distance between the stationary marker and the spring marker; however, in this investigation it was found that consistent results were obtained by using the spring marker only. The criterion for judging this was the agreement between weight change during a run as measured by the spring and weight change during a run as measured by the microbalance.

A static assembly attached to the reaction tube and consisting of winch, nylon thread, platinum wire, quartz rod and platinum hook was used for oxidizing specimens when kinetic data were not required. This apparatus had the advantage of being able to handle up to four specimens simultaneously.

Figure 3-3 Calibration of Ni-Span-C Spring

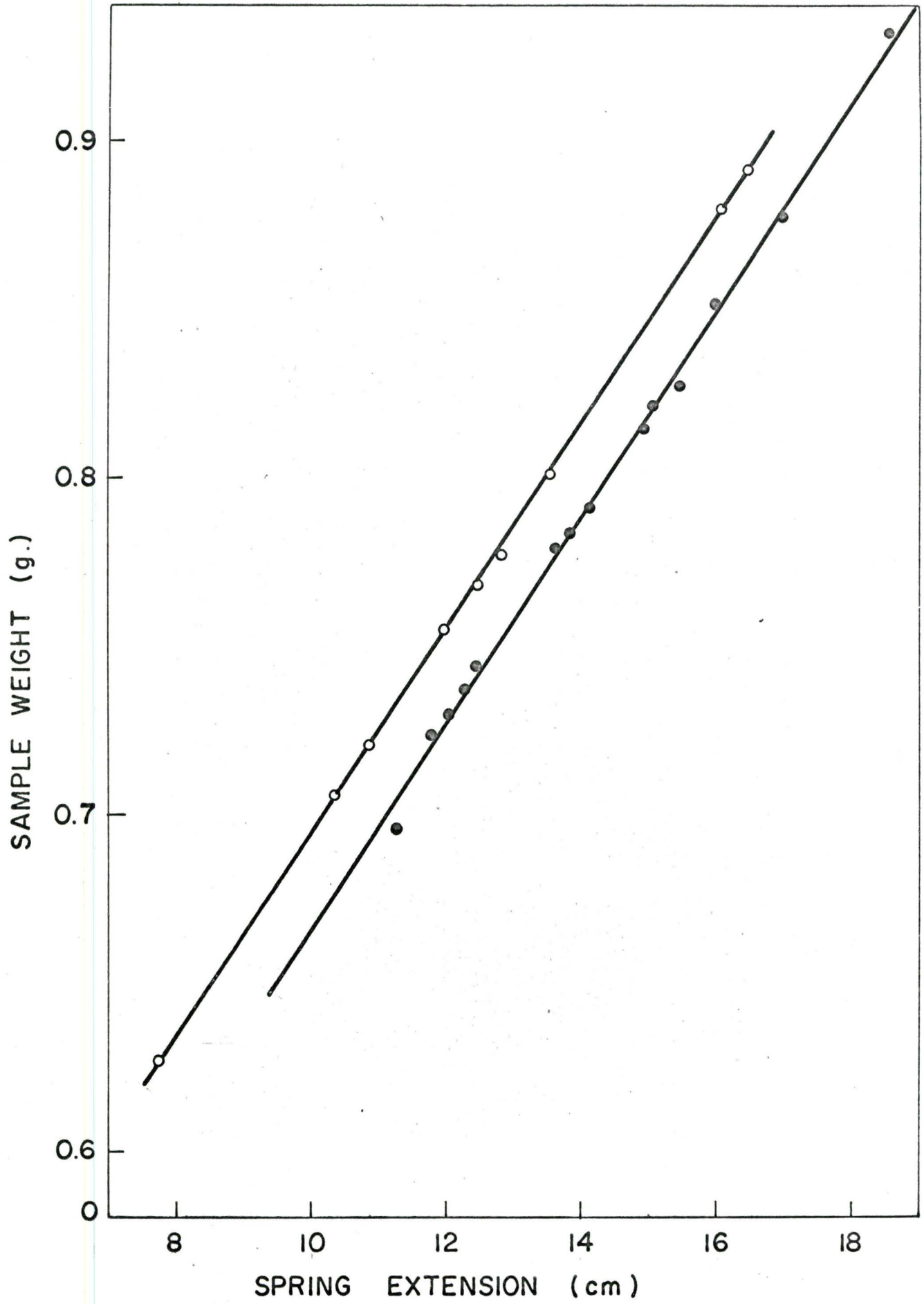

All oxidation and decarburization tests were carried out at a temperature of 950°C.

3.2 Experimental Procedure

3.2.1 Specimen Preparation

Most workers in the field of oxidation tend to use foils or thin sheets for specimens, in order to have as large a surface area as possible without making the weight of a specimen excessive. It was decided to use thicker specimens in this investigation, since diffusion of carbon in the metal is an important factor, and diffusion rates are quite high.

The iron-carbon alloys were obtained from Dr. G. R. Purdy, McMaster University as bars of the homogenized alloys at various carbon compositions. Two alloys were used, Fe-0.218%C and Fe-0.810%C. Metallographic examination of the as-received material showed slight surface oxidation and decarburization. This was eliminated by removing approximately 1.5 mm. from the surface of the bar. Specimens were then cut directly from the bar into rectangular solids of approximately 7 mm. x 5 mm. x 3 mm. A hole of approximately 1 mm. diameter was drilled to suspend the specimens in the kinetic assembly. The samples were mounted in bakelite and polished on all sides through 220, 320, 400 and 600 silicon carbide papers under water as a lubricant. Final polishing was done on selvyt cloths

impregnated with 6μ and 1μ diamond abrasive. After removal from the bakelite, they were washed with petroleum ether and acetone. The dimensions were measured with a micrometer to the nearest 0.01 mm. and the surface area computed. A typical specimen had a surface area of approximately 1.5 cm^2 and a weight of approximately 0.8 gm. Immediately before a test the samples were washed again with petroleum ether and acetone and weighed accurately on the microbalance. At all times after the final polishing, samples were handled with chrome-plated tweezers to minimize contamination of the polished surfaces.

3.2.2 Reactions

Samples prepared as described above were suspended on the platinum hook in the kinetic assembly, which was then connected to the top of the furnace. The system was evacuated with the mechanical pump for at least one hour and the furnace raised to operating temperature. It was then flushed with prepurified nitrogen and the reaction gas (usually pure CO_2) was allowed to flow for about an hour. At the end of this time the sample was then lowered into the hot zone of the furnace and cathetometer readings were taken as soon as possible. Usually the first reading was obtained two or three minutes after lowering the sample and for the purpose of recording the kinetic data, this was considered as time zero. Readings were

converted into oxygen uptake per unit area, $\frac{\Delta m}{A}$, by using the relationship

$$\frac{\Delta m}{A} = \Delta \ell \frac{k}{A} \tag{36}$$

where $\Delta \ell$ is the difference in cathetometer reading from zero point (cm),

k is the spring constant = 30.5 mg/cm, and

A is the surface area of specimen (cm^2).

The cathetometer could be read to ± 0.003 cm, which corresponds to a precision in $\Delta m/A$ of about ± 0.06 mg/cm^2 for a typical specimen.

During reaction with CO_2, both wustite formation and decarburization occur simultaneously. After forming a layer of wustite on the surface, the next step was to stop the oxidation and allow the decarburization to proceed by reaction of carbon with wustite,

$$C + FeO \rightarrow Fe + CO \tag{37}$$

Two methods of doing this were tried: (1) to evacuate the system and allow the above reaction to proceed in a vacuum and (2) to replace the CO_2 with argon. In the first case the gas supply was turned off and stopcocks closed at the inlet and outlet of the furnace. The system was then evacuated using the mechanical pump and the diffusion pump to a pressure of the order of 10^{-3} mm. Hg and readings

were continued as soon as possible after changing the conditions. After the run was over, the system was brought back to atmospheric pressure by admitting prepurified nitrogen. The sample was then raised out of the furnace and allowed to cool. After the reaction, the sample was used for either carbon analysis or metallography. In the second case, the CO_2 was shut off and argon turned on without any intermediate evacuation of the system. After the reaction, the weight change was rechecked using the microbalance, except in a few cases where it was obvious that some of the oxide had spalled off, or where a piece of the platinum wire became imbedded in the oxide.

3.2.3 Metallography

Specimens were mounted in cold mount resin as recommended by Jay [41], rather than in bakelite, which tends to cause the scale to break away from the metal. They were polished through 220, 320, 400 and 600 silicon carbide papers, with final polishing on 6μ and 1μ diamond-impregnated cloths. Where etching of the metal surface was employed, the etchant was 2% nital. Both cross sections and tapered sections through the oxide layer were used. Surface topography was examined directly, without mounting the oxidized samples.

3.2.4 Carbon Analyses of Scaled Samples

The wustite layer was removed by pickling in dilute HCl (1:4) at room temperature until visual examination showed complete removal of oxide. The specimens were then washed with distilled water, acetone and petroleum ether, dried and weighed. It was established that the loss of metal by this pickling procedure was very small. Carbon analysis was carried out by combustion of the entire specimen and suitable corrections were applied for temperature and pressure.

CHAPTER IV

EXPERIMENTAL RESULTS

4.1 Introduction

In this section, the kinetics of oxidation and decarburization experiments will be presented as plots of $\Delta m/A$ against t. $\Delta m/A$ is expressed in mg/cm^2, and time in minutes. Upon exposure of a specimen to the oxidizing atmosphere, its change of weight is caused by a combination of oxygen uptake by wustite formation and carbon loss by oxidation to carbon monoxide. The results of carbon analyses of specimens reacted under various conditions will be shown, as well as photomicrographs illustrating structural features of the metal and the oxide scale.

4.2 Oxidation Kinetics

Typical oxidation curves for Fe -0.8%C in pure CO_2 at $950^{\circ}C$ are shown in Figure 4-1. The initial slope of a curve was usually positive, but a negative initial slope was observed in a few cases. In previous research by Billings[25], the initial slope in pure CO_2 was observed to

Figure 4-1 Oxidation Kinetics of Fe-0.8%C in CO_2 at 950°C

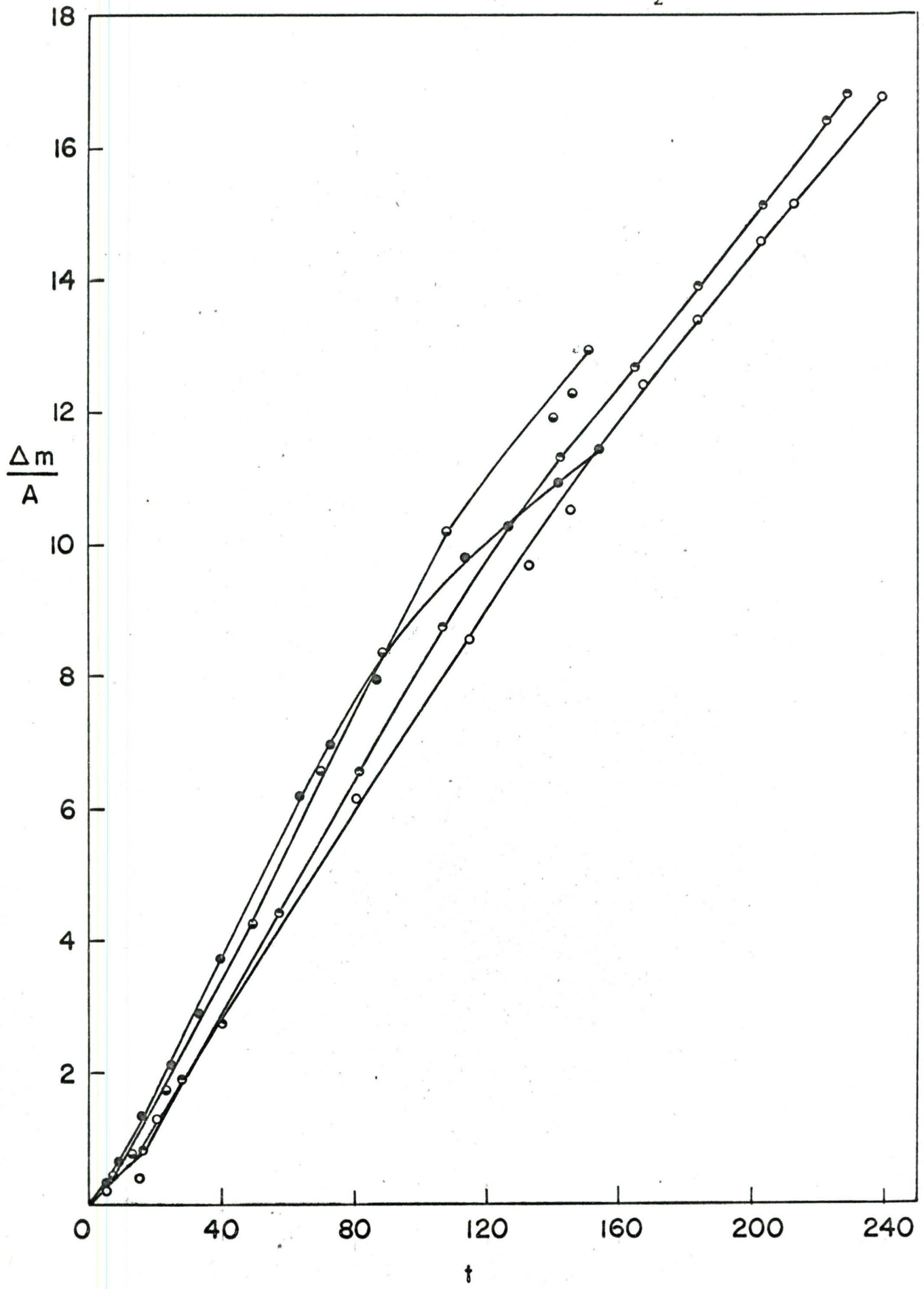

be positive for Fe -0.6%C, and negative for Fe -1.1%C. The present work gives values for the initial slopes which are intermediate between his values. The linear rate constant as observed from the data in Figure 4-1 is 0.093 ± 0.012 $mg/cm^2/min$. The linear rate constant decreases at long experimental times and eventually the kinetic curve tends to become parabolic.

Oxidation tests were also carried out at a CO_2 partial pressure of 400 mm and 200 mm, both at one atmosphere total pressure with the remaining gas being argon, and at reduced pressure with no other gas present. At P_{CO_2} = 400 mm a two-stage linear process is observed, and there appears to be no difference between the second linear rate constant observed with or without argon present. The work of Pettit, Yinger and Wagner[16] indicates that the second linear rate is associated with the growth of the scale, while the first linear stage is associated with oxide nucleation, and may depend on the grain size of the metal. As these investigators have shown for the oxidation of iron, argon acts only as a diluent in the atmosphere and the oxidation of the Fe-C alloy was identical in atmospheres of the same CO_2 partial pressure.

The purpose of these experiments was to determine if microporosity in the oxide scale had any effect on rate of carbon removal, if the pores were of such a size that the presence of large argon molecules could partially

Figure 4-2 Oxidation Kinetics of Fe-0.8%C at P_{CO_2} = 400 mm

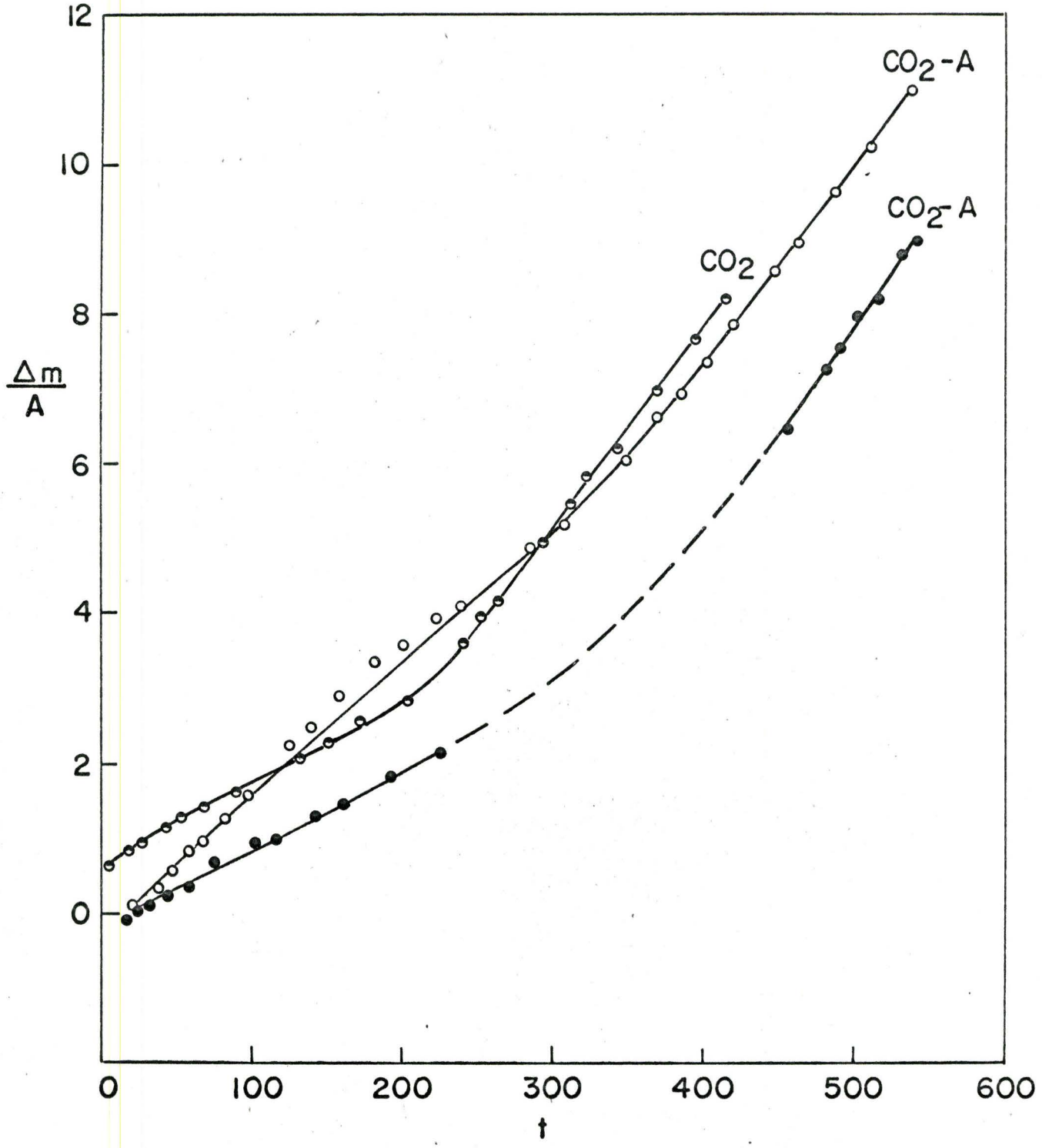

Figure 4-3 Oxidation Kinetics of Fe-0.8%C at P_{CO_2} = 200 mm

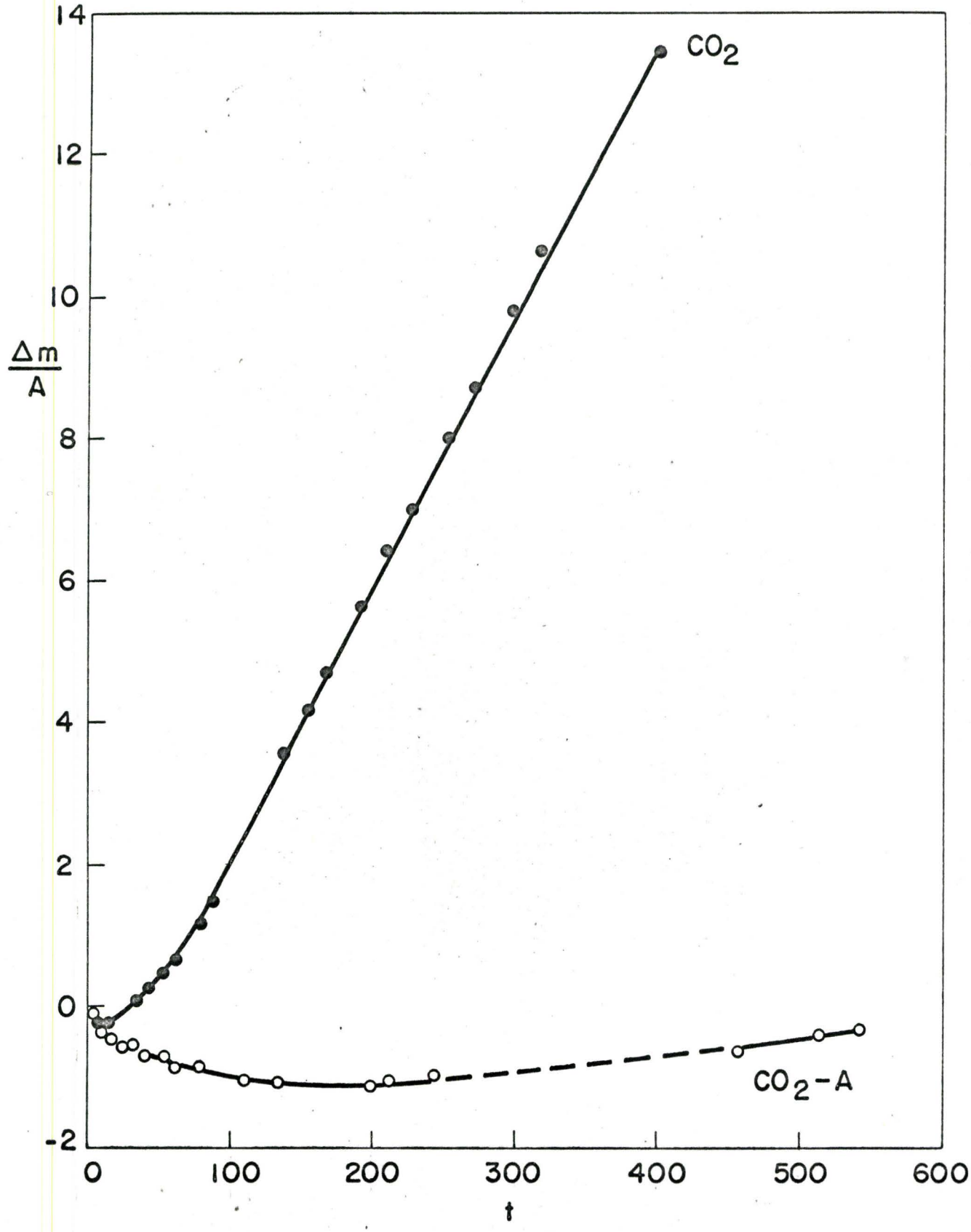

block the passage of carbon dioxide through the scale. The linear rate constants, Figure 4-2, observed at P_{CO_2} = 400 mm were .028 ± .001 mg/cm^2/min. (The errors quoted are standard deviations.) At P_{CO_2} = 200 mm, the initial stages of the reaction curves showed a weight loss due to decarburization, and subsequent change to weight gain as wustite formation progressed. These results are presented in Figure 4-3. At this lower CO_2 partial pressure, the curves for specimens exposed in different atmospheres are of distinctly different magnitude. No explanation can be offered for the large difference in the two curves, one at atmospheric pressure in a CO_2-argon mixture and the other at reduced pressure in pure CO_2.

4.3 Decarburization Kinetics

4.3.1 Vacuum Decarburization

Immediately after shutting off the CO_2 supply and allowing a scaled specimen to react under vacuum, an abrupt change from weight increase to weight decrease was observed, indicating loss of carbon from the specimen. The results are shown in Figures 4-4 to 4-6. For clarity the oxidation step is shown in only one case to give a typical representation of a complete experimental test. The loss of carbon from a specimen became continuously slower with increasing exposure time. The rate of carbon loss appears to be a function of the thickness of the oxide layer,

Figure 4-4 Kinetics of Vacuum Decarburization at 950°C following immediately after oxidation in CO_2

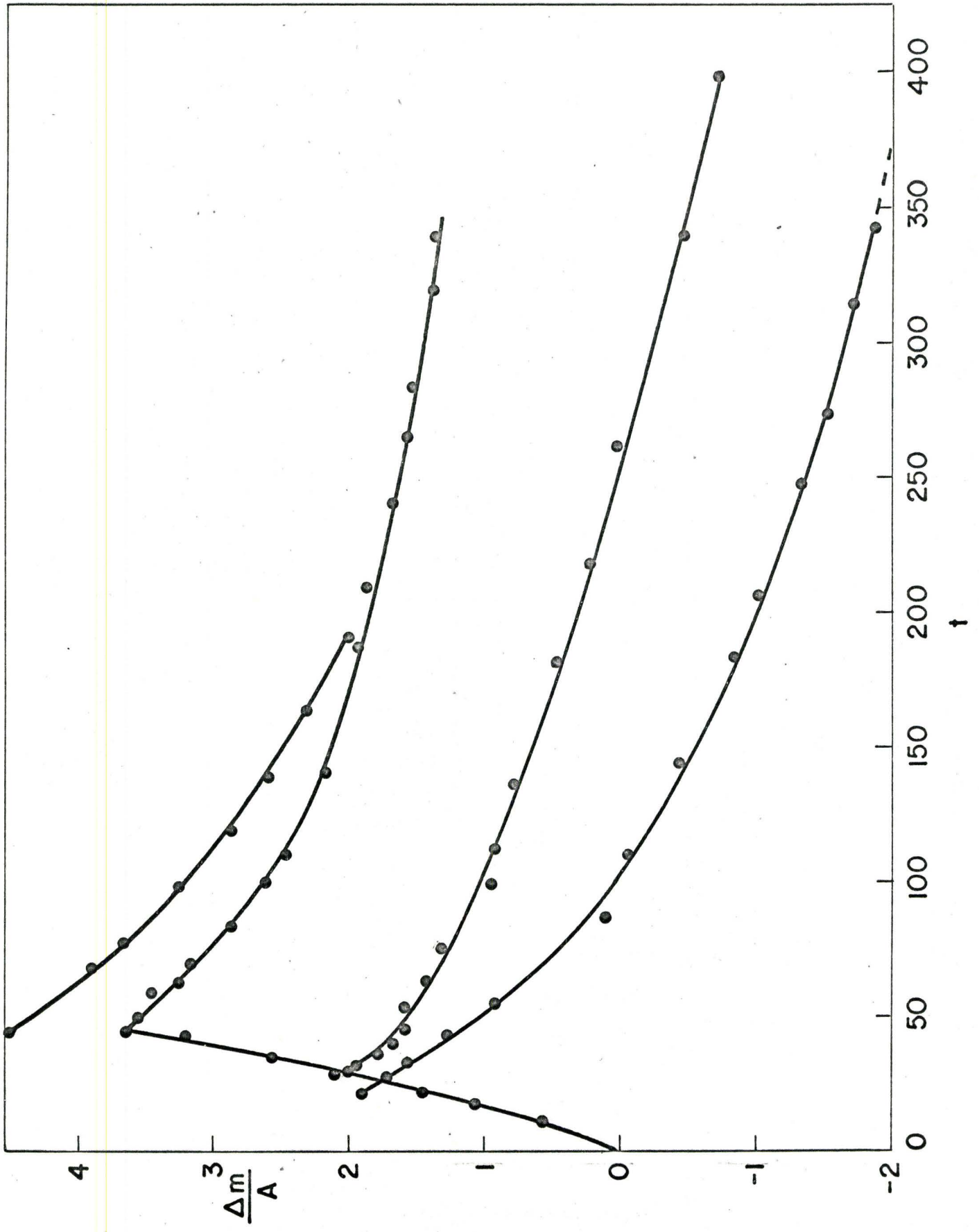

Figure 4-5 Kinetics of Vacuum Decarburization at 950°C

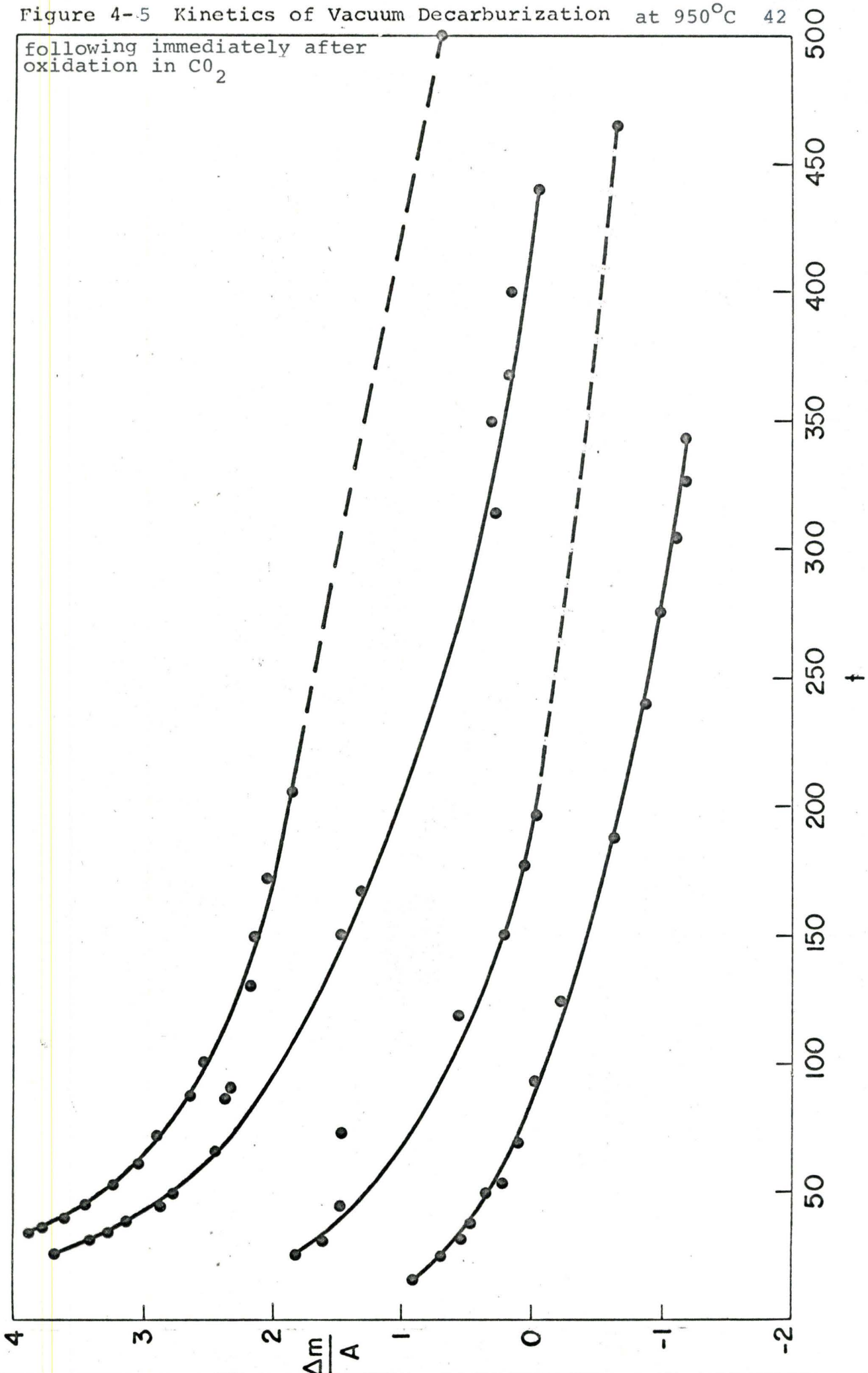

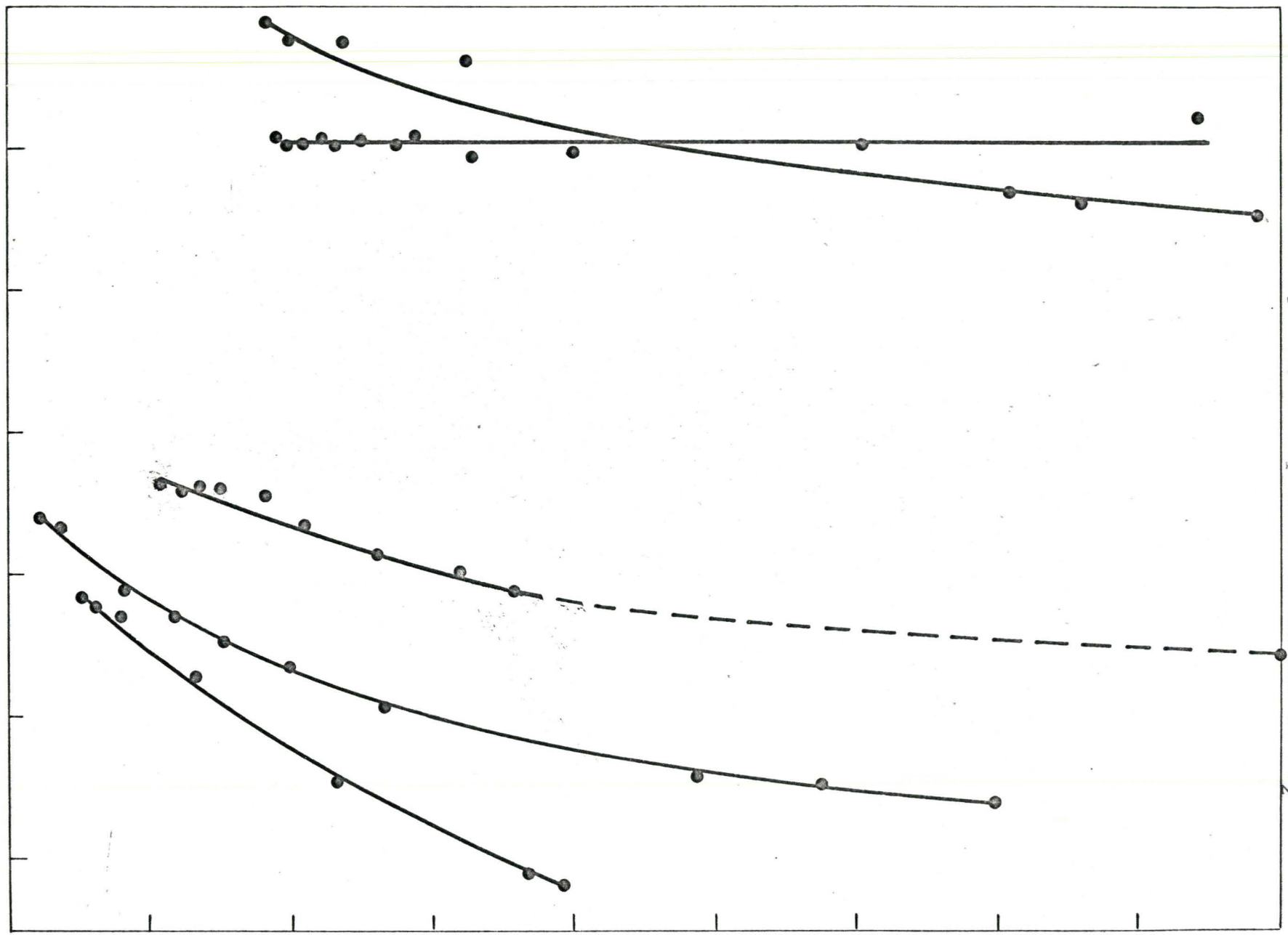

Figure 4-6 Kinetics of Vacuum Decarburization at 950°C following immediately after oxidation in CO_2

decreasing as the oxide thickness is increased. With very thick oxide scales, approximately 100 μ thick decarburization was not observed during the time of the experiments.

4.3.2 Decarburization in an Argon Atmosphere

When the gas flowing through the apparatus was changed from CO_2 to argon, a period of about twenty minutes was required to flush all the CO_2 from the system. During this period a continuously decreasing oxidation rate would be expected, until all CO_2 was removed, and then decarburization according to equation 37 should be the only reaction observed. The curves showed a slight increase in oxidation rate immediately after admission of argon to the system, followed by a decreasing rate, and eventually a decrease in weight due to decarburization. The decarburization kinetics appear to be similar to those observed under vacuum. The results of these experiments are presented in Figure 4-7.

4.4 Carbon Analyses

Samples oxidized in pure CO_2 for varying periods of time were prepared as described in Section 3.2.4 and analyzed for residual carbon content. Figure 4-8 shows the carbon loss as a function of time during the oxidation period. After an initial period of rapid carbon loss, a linear rate is obtained. The slope of the linear portion

Figure 4-7 Kinetics of oxidation in CO_2, followed by reduction of oxide in argon atmosphere

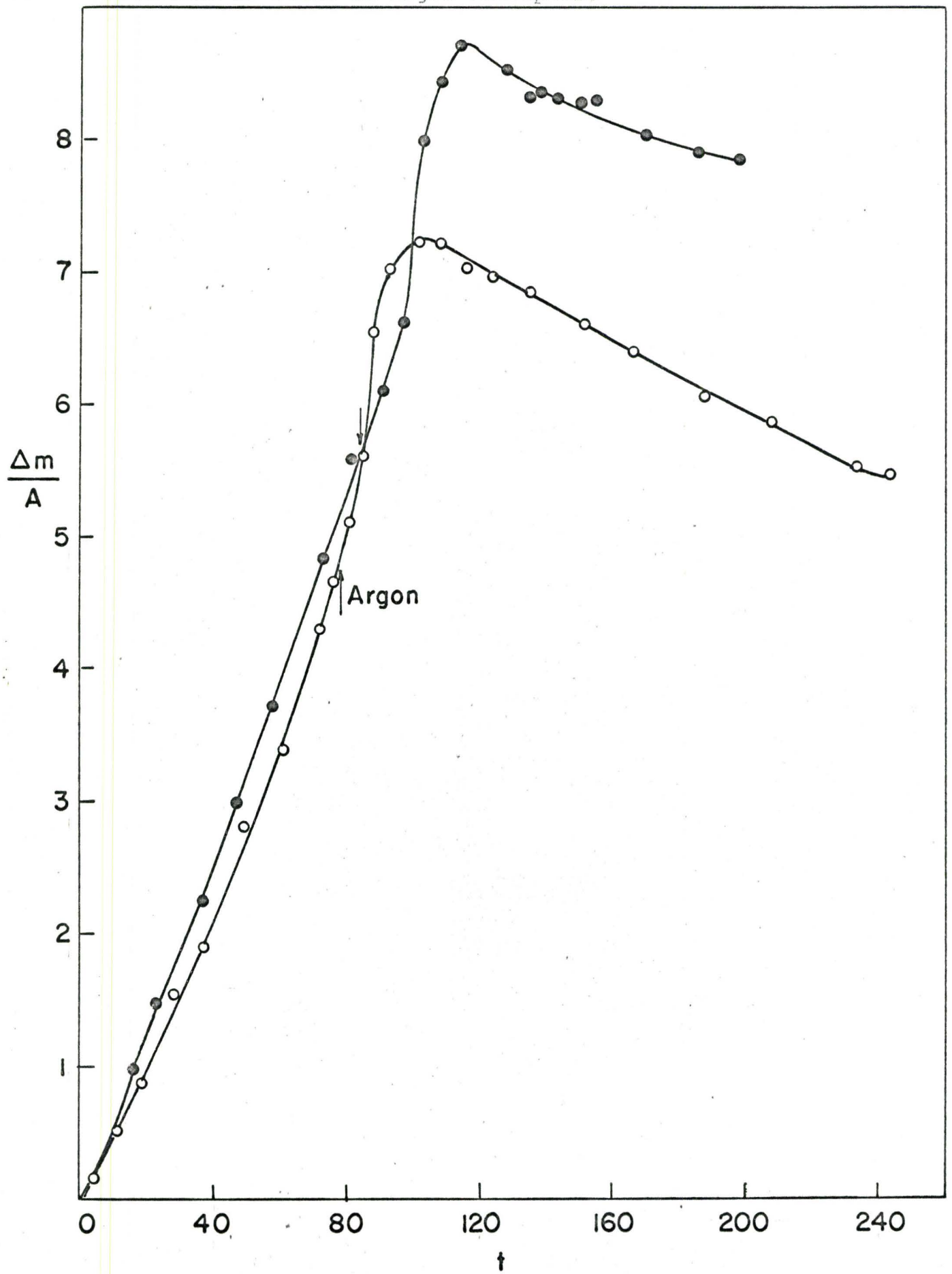

of the curve is 6.0×10^{-3} mg/cm^2/min. Microscopic examination of the wustite scales illustrated that the onset of the linear rate corresponded approximately to complete coverage of the metal surface with oxide. The carbon loss corresponding to complete decarburization of the specimen varies slightly with the geometry of the specimen, but would generally be about 4.5 mg/cm^2.

In another series of experiments, the oxidation time in pure CO_2 was kept constant at 90 min. The specimens were then decarburized under vacuum for varying periods of time and analyzed for residual carbon. The results, as shown in Figure 4-9, indicate that decarburization by oxide reduction proceeds more slowly than decarburization in a CO_2 atmosphere.

4.5 Metallography

4.5.1 Surface Appearance

After long periods of oxidation (i.e., greater than 30-40 min.) the metal surface appeared to be entirely covered with oxide crystallites. Since the crystal structure of wustite is cubic, it is not suprising that square or rectangular faces are most frequently observed. Triangular faces, possibly from growth of the octahedral planes, are observed less frequently.

Figure 4-8 Carbon Loss During Oxidation in CO_2

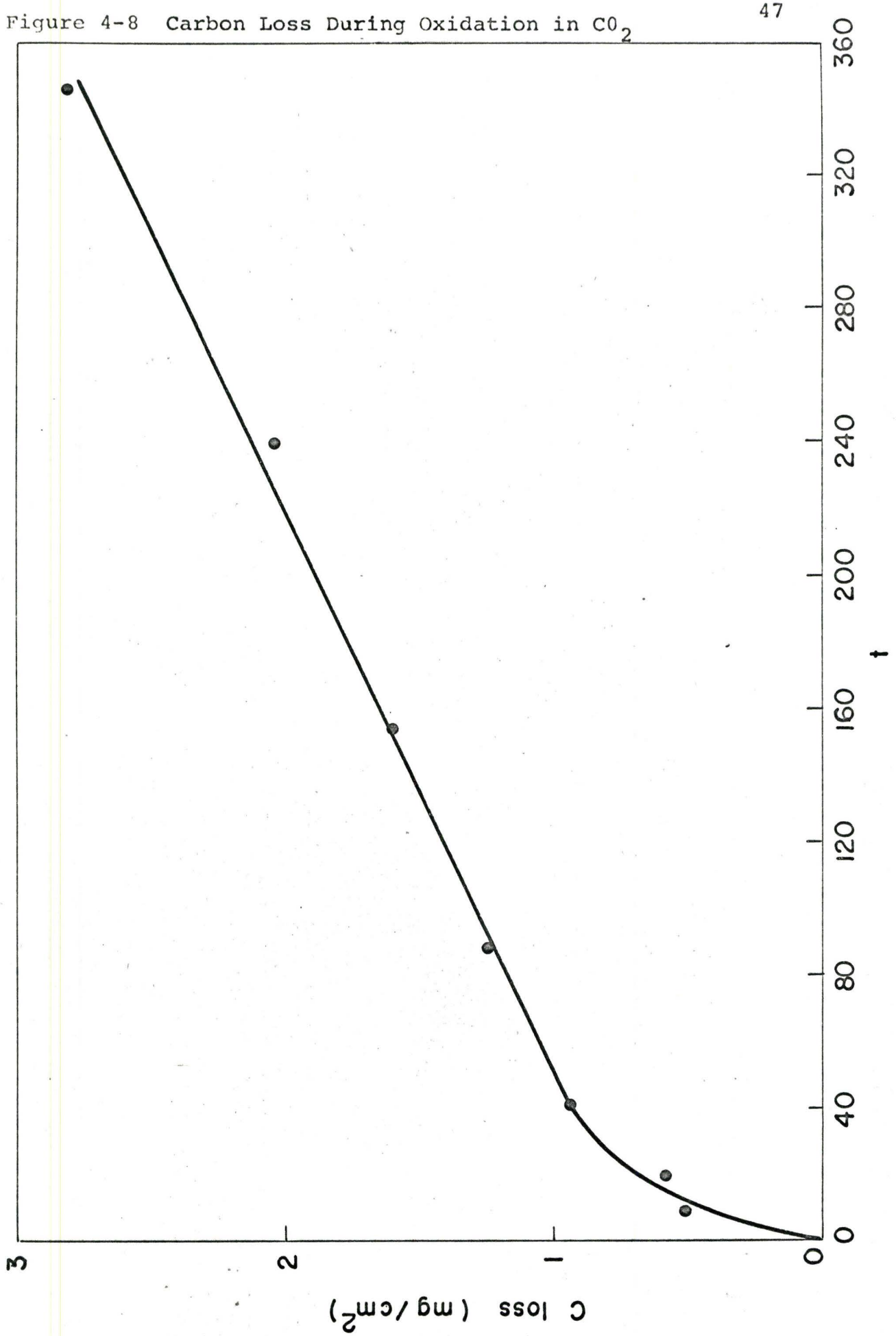

Figure 4-9 Carbon Loss During Vacuum Decarburization, with prior oxidation time constant at 90 min

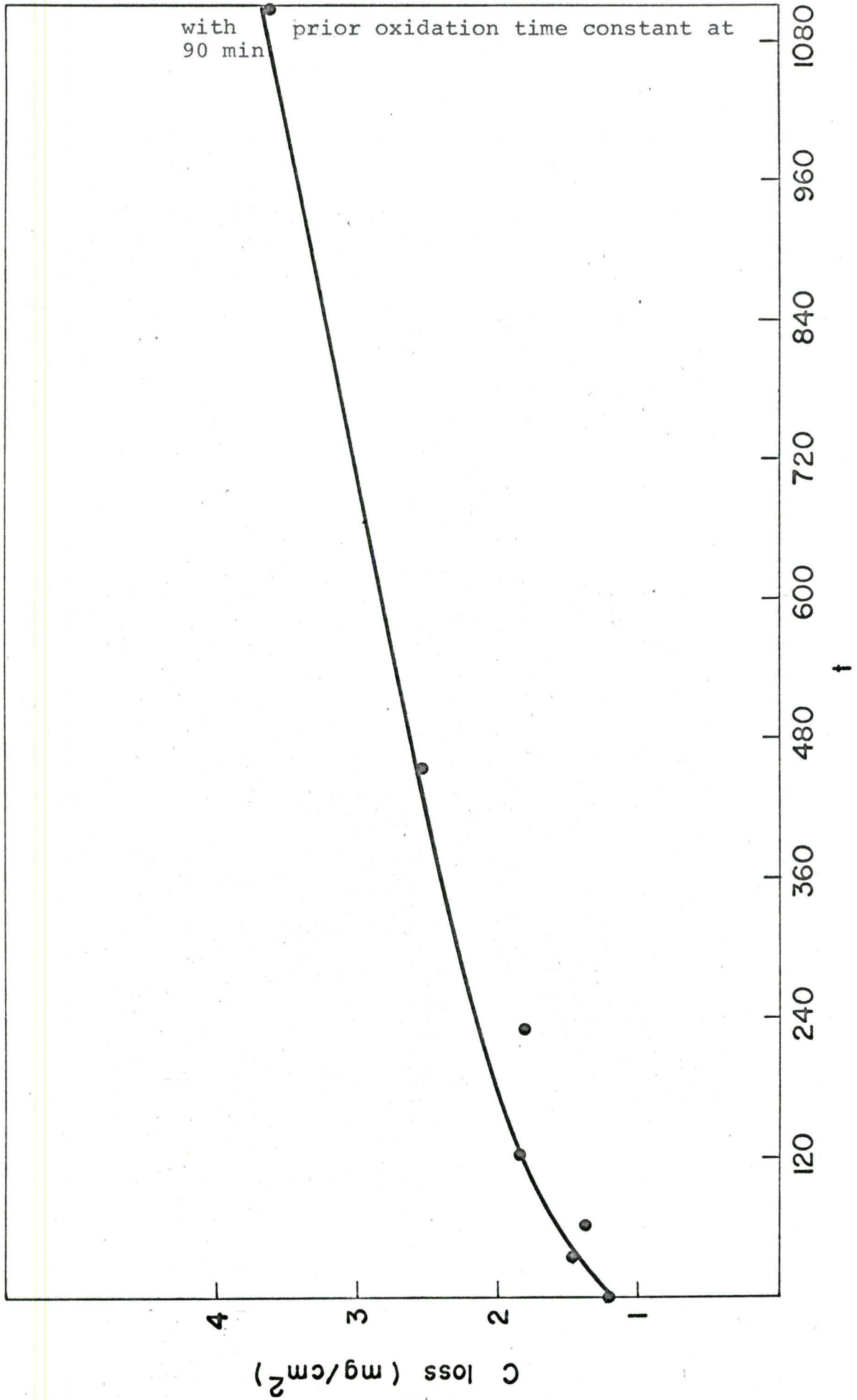

The growth of crystallites was very irregular, as shown by the variation in crystallite size on the same specimen, and the presence of a large number of ledges and kinks on the crystallite surfaces. The general trend was toward larger size crystallites as the oxide layer thickened. These features are illustrated in Figures 4-10 to 4-12.

During decarburization, under vacuum or in an inert gas atmosphere, the oxide was reduced to metal. This results in a patchy appearance showing areas of metal protruding where the oxide has been reduced. The exposed metal surface is very irregular, as the reaction of oxide with carbon also involves formation of voids due to the difference in volume between the oxide and the metal. A typical specimen is shown in Figure 4-13. This type of appearance was observed only on samples having a relatively thin oxide layer, but the same type of behaviour would be expected to occur with thick oxide layers after extremely long times.

4.5.2 The Metal-Oxide Interface

During oxidation in pure CO_2, the oxide was usually quite adherent to the metal, as shown in Figure 4-14. Sometimes, however, it appears that a reaction of carbon with wustite occurs at the metal-oxide interface with the result that voids are formed, and iron precipitated at the interface, as shown in Figures 4-15 and 4-16.

Figure 4-10 Surface Topography, Oxidation Time in CO_2 18 min. x 150

Figure 4-11 Surface Topography, Oxidation Time in CO_2 36 min. x 150

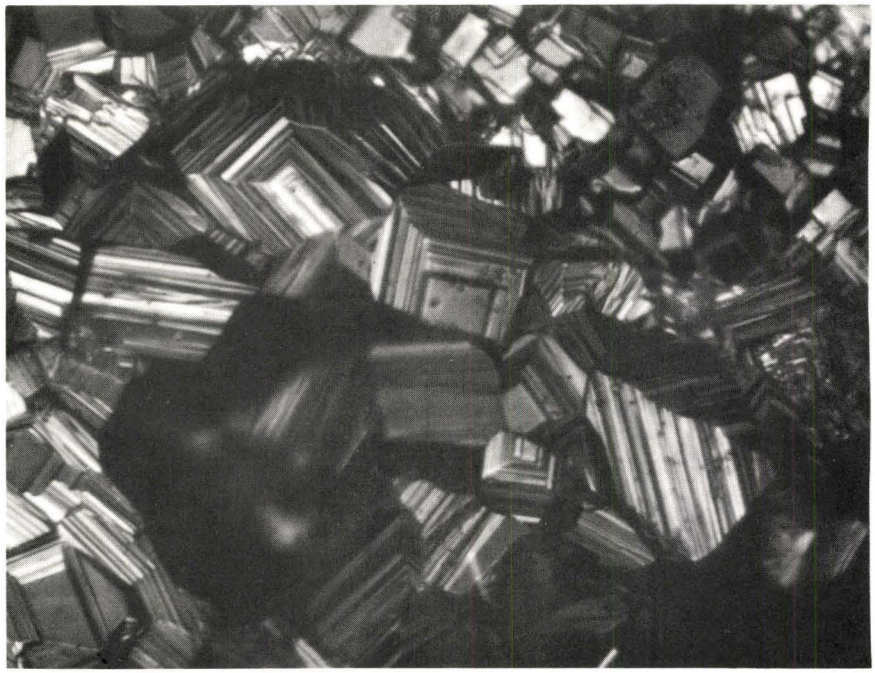

Figure 4-12 Surface Topography, Oxidation Time in CO_2-Argon (P_{CO_2} = 400 mm.) 540 min. x 150

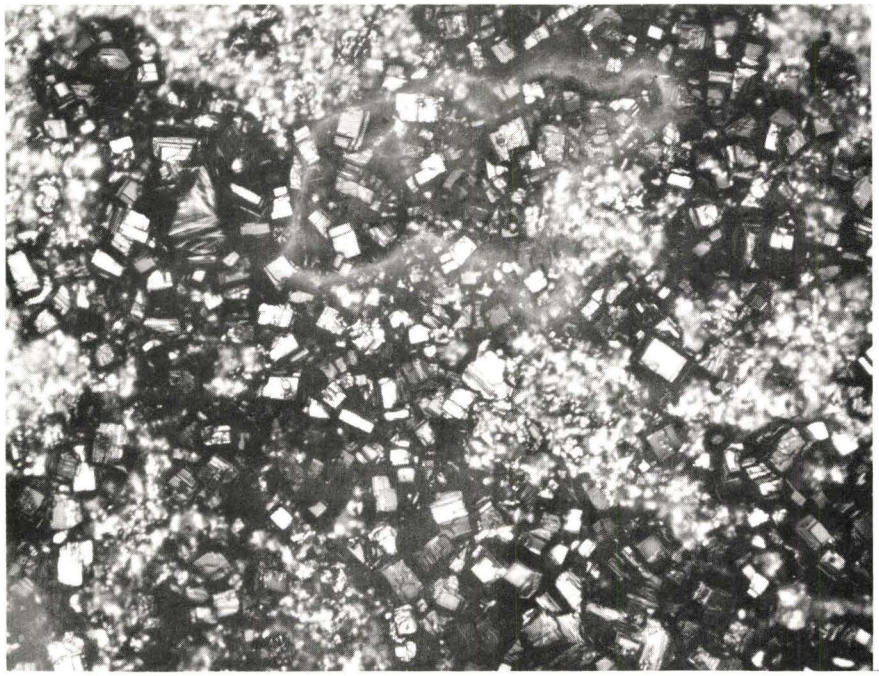

Figure 4-13 Surface Topography, Oxidation Time in CO_2 23 min., Vacuum Decarburization Time 141 min. x 150. Light areas indicate reduction of oxide to metal.

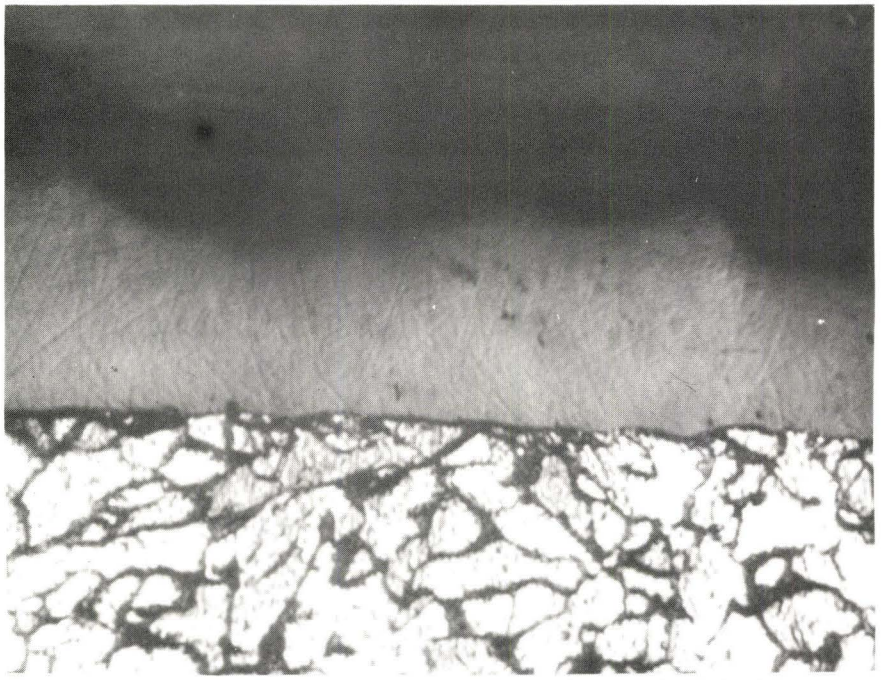

Figure 4-14 Metal-Oxide Interface After Oxidation in CO_2. x 200

Figure 4-15 Void Formation and Iron Precipitation at Metal-Oxide Interface After Oxidation in CO_2 (unetched). x 380

Void formation and iron precipitation become even more prominent when an oxidized sample was allowed to decarburize under vacuum or in an inert gas atmosphere. As shown in Figure 4-17, the metal-oxide interface is extremely irregular as the oxide becomes reduced, and voids are formed at the interface. By measuring the relative areas of voids (dark) and metal (light) it is estimated that the void volume at the interface (39%) is of the same order of magnitude as the difference in volume of the metal and the oxide (43%). The gas formed in this reaction must pass through the scale, and it is believed that there is enough porosity between crystallites and along the kinks and ledges in the crystallites to enable the gas to escape.

Thinner oxides can be completely reduced in some places by the decarburization reaction, as shown in Figures 4-18 to 4-20, exposing areas of reduced metal (compare with Figure 4-13). Passage of carbon through the oxide is indicated by the reduced iron left behind. (Fig. 4-18.) Figure 4-19 shows the presence of iron "spires" extending through, or almost through the oxide layer. The same effect can be seen by taper-section metallography; an example is presented in Figure 4-21. Figure 4-22 is a schematic diagram of the method used in observing tapered sections.

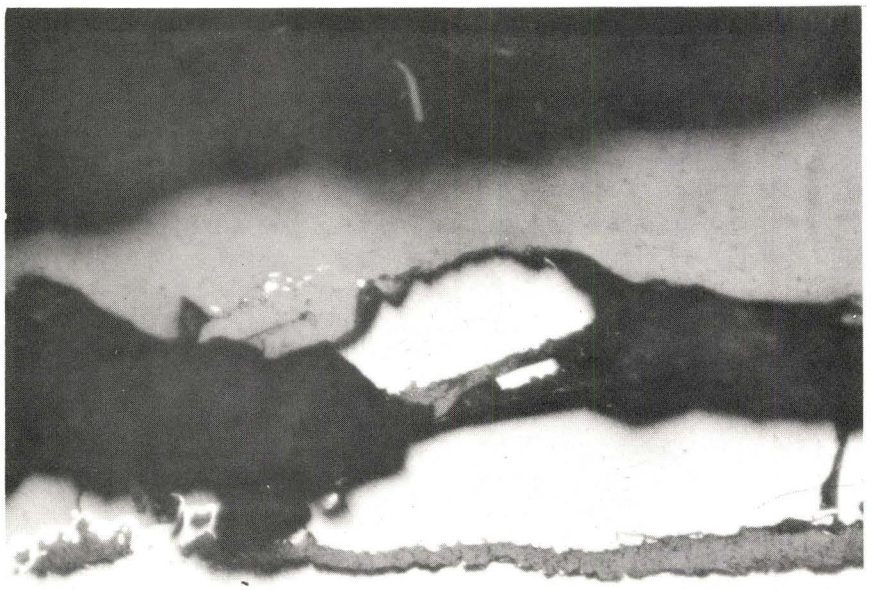

Figure 4-16 Void Formation and Iron Precipitation at Metal-Oxide Interface After Oxidation in CO_2-Argon (unetched). x 400

Figure 4-17 Void Formation and Iron Precipitation at Metal-Oxide Interface After Vacuum Decarburization for 3 hr. Void fraction at metal-oxide interface is 39%. x 400

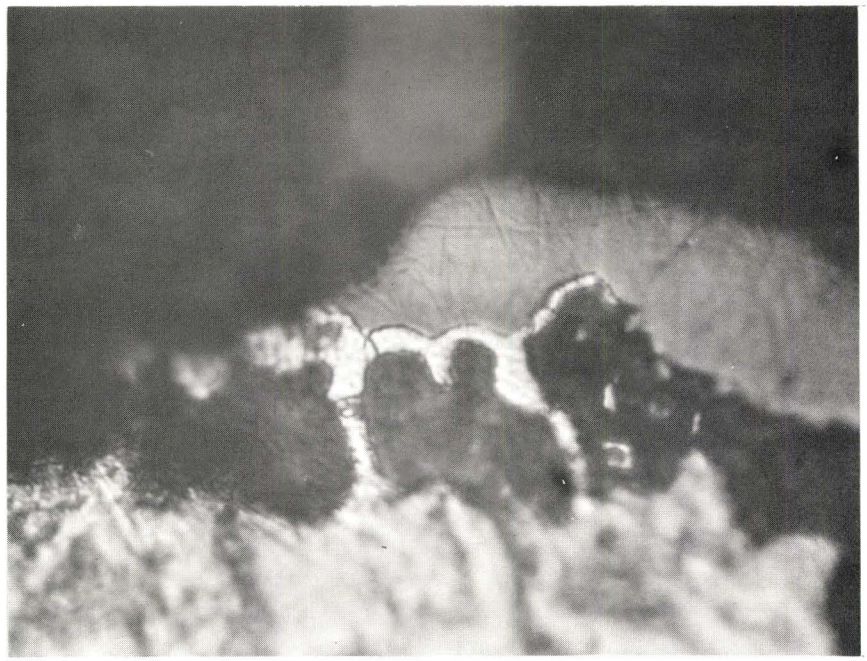

Figure 4-18 Complete Reduction of Oxide During Vacuum Decarburization. x 250

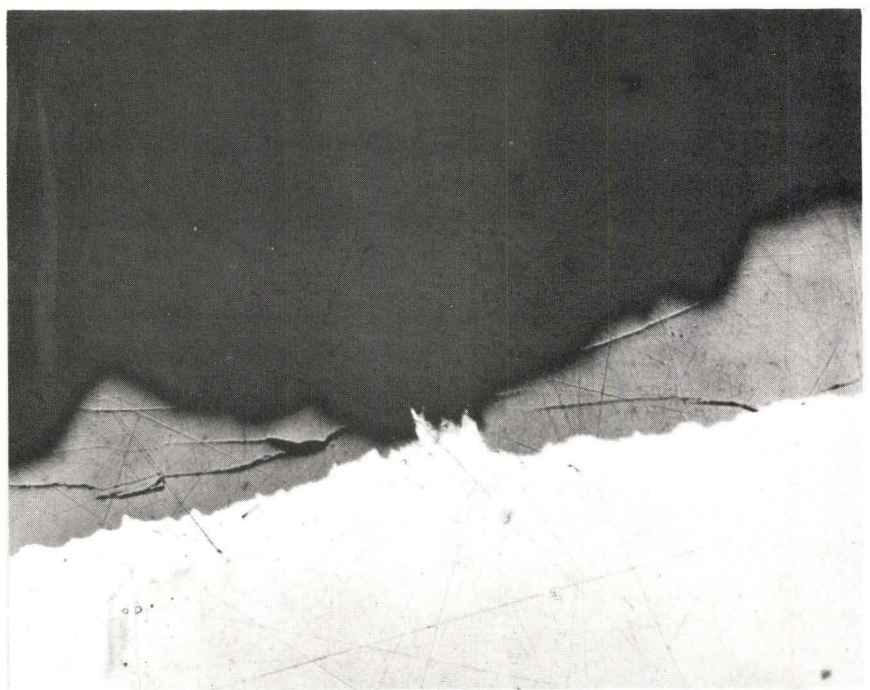

Figure 4-19 Complete Reduction of Oxide During Decarburization in Argon for 7 hr. Iron "spires" are associated with oxide porosity. x 170

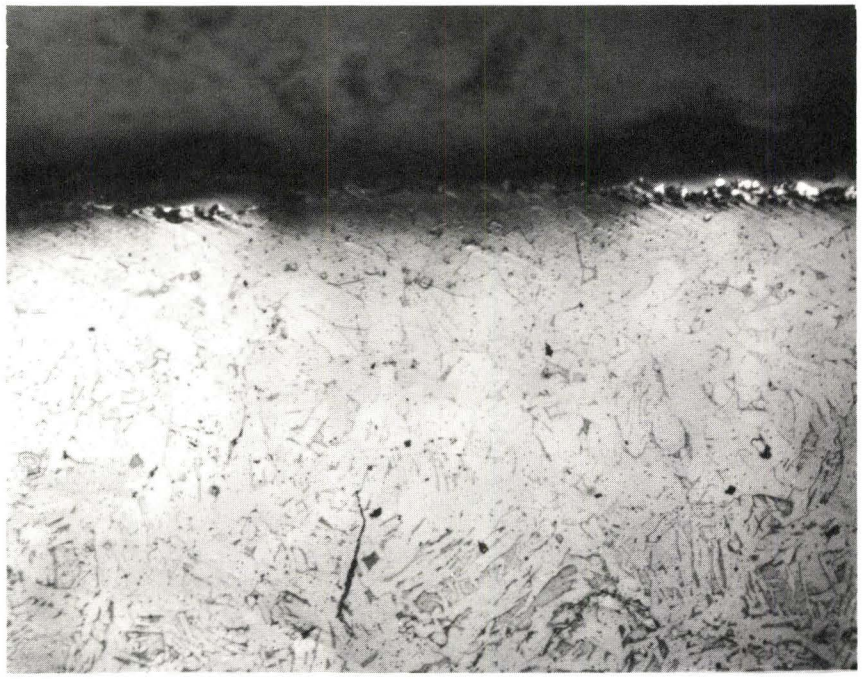

Figure 4-20 Complete Reduction of Oxide During Vacuum Decarburization. x 200

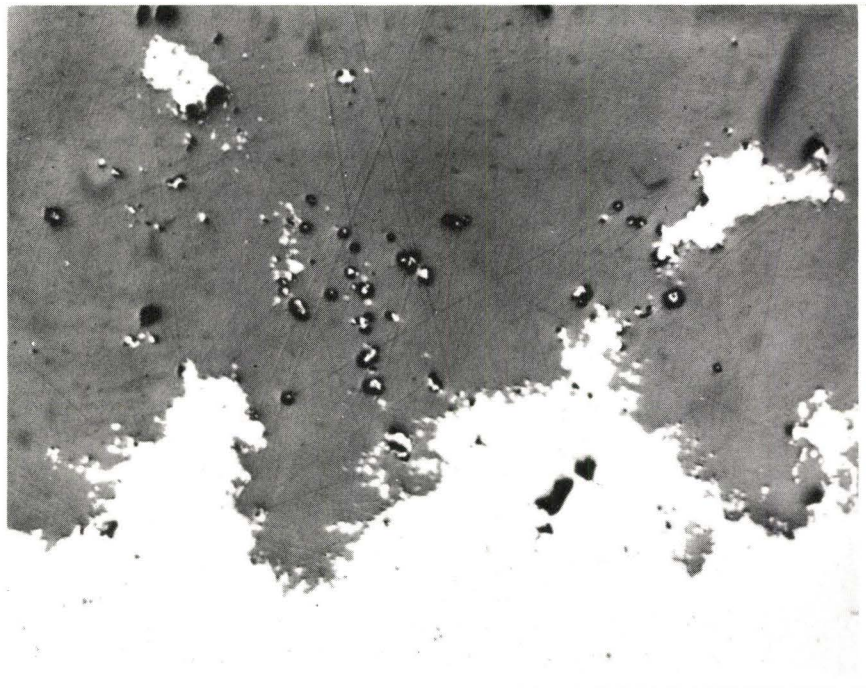

Figure 4-21 Reduction of Oxide During Decarburization in Argon, Tapered Section (unetched). x 170. Iron precipitation in oxide is associated with oxide porosity.

FIGURE 4-22

Schematic Diagram of Tapered Section Metallography

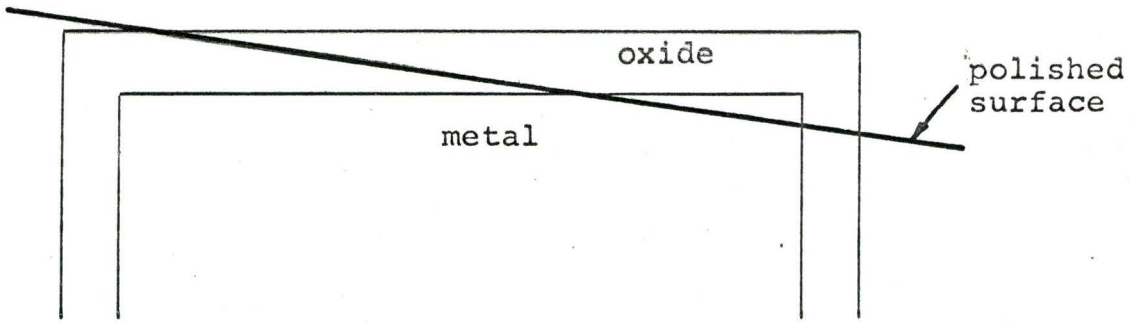

In addition to porosity in the scale, it was evident that some blistering or cracking of the scale occured. If the oxide layer is dense and pore-free, a buildup of carbon could occur just beneath the metal-oxide interface.[33] Reaction of carbon with the oxide could then result in formation of a bubble of carbon monoxide, which would rupture the scale when the pressure became sufficiently high. Figures 4-23 and 4-24, taken from a tapered section of the same sample suggest this possibility. Figure 4-23 shows an area of high carbon content surrounded by an area of extensive decarburization. In Figure 4-24, the scale appears to be ruptured, and the dark etching of the underlying metal suggests that this may be a high-carbon area.

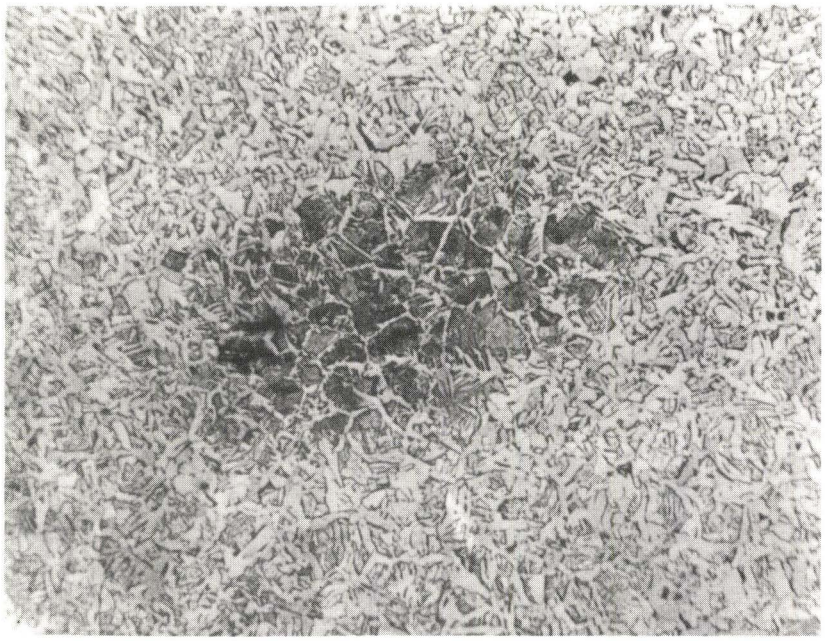

Figure 4-23 Metal Surface of Non-Uniform Carbon Content, Tapered Section. x 100 This structure is associated with blister formation.

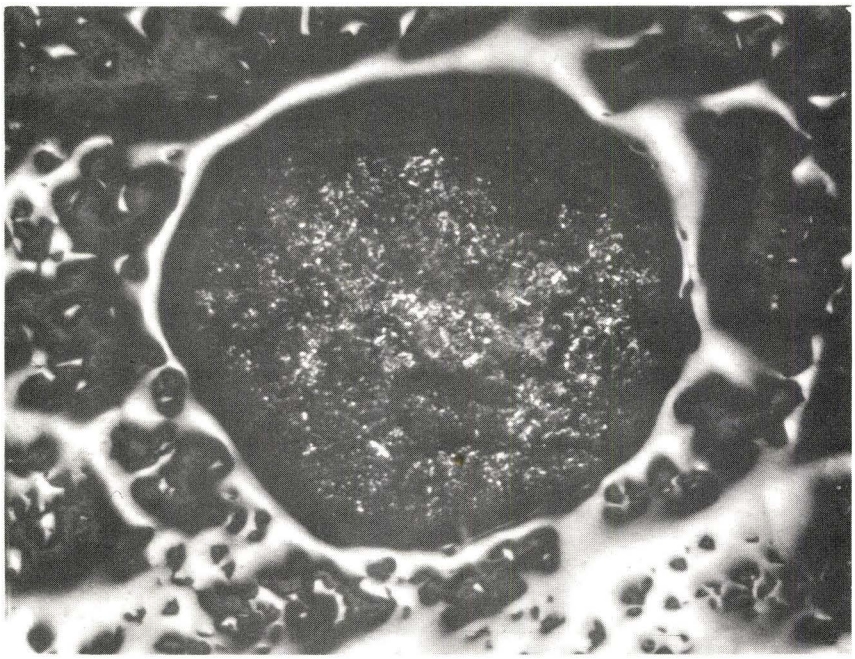

Figure 4.24 Blistering of Oxide, Tapered Section. x 100 . The central area of the blister is underlying metal surface.

The mechanisms of porosity and blistering as possible means of transport of carbon through the oxide will be discussed more fully in Chapter 5.

4.5.3 Metal Structure

The original alloy, Fe-0.810%C, is very close to the eutectoid composition, and showed a structure which was almost entirely pearlitic. After decarburization of about 6 hours following a preliminary oxidation period of one-half hour in CO_2, incipient decarburization in the form of Widmanstatten plates of ferrite is observed at the center of the specimen (about 1.5 mm from the surface) and more extensive decarburization is seen near the surface, as may be seen in Figures 4.25 and 4.20. These results are similar to those of other workers, e.g., Engell[27].

Figure 4-25 Incipient Decarburization at Center of Specimen. x 150

CHAPTER V

DISCUSSION

5.1 Oxidation of the Fe 0.8%C Alloy in Carbon Dioxide

5.1.1 Oxidation of Iron in CO_2

By considering the observed weight changes to be the sum of the partial reactions of iron oxidation and carbon oxidation, it should be possible to estimate the total oxygen uptake, and thus determine if the presence of carbon in the alloy has a marked effect on the rate of iron oxidation. During the initial stages of oxidation, wustite formation is relatively slow, and carbon loss is relatively rapid, in comparison with later observations. This is the "first linear stage" of Pettit et al.[16] where nucleation of FeO and its epitaxial relationships with the underlying metal are significant and give rise to erratic kinetics. Also, the rate of carbon oxidation continuously decreased and was dependent on the surface coverage of oxide. For these reasons, the evaluation of the oxidation rate of iron in the alloy was difficult. However, the oxidation kinetics became approximately of constant rate after the first half hour.

For oxidation times greater than about 30 minutes, linear curves of total weight change and of carbon loss are more clearly defined. From Figure 4-1, a linear weight gain of .093 ± .012 mg/cm^2/min is observed, corresponding to both iron and carbon oxidation. Also from Figure 4-8, the rate of carbon loss is .006 mg/cm^2/min, corresponding to an oxygen uptake due to carbon oxidation of .008 mg/cm^2/min, assuming that the reaction product is CO. Thus k_ℓ for wustite formation was .101 ± .012 mg/cm^2/min. This is in good agreement with the rate observed by Billings[25] for oxidation of iron-carbon alloys in pure CO_2, and also in reasonably good agreement with the data of Smeltzer[15] for pure iron oxidized in CO_2. It appears that in pure CO_2, the oxidation rate of iron is not significantly affected by alloying with 0.8% carbon.

5.1.2 Oxidation of Carbon in CO_2

According to Figure 4-8, carbon oxidation proceeds rapidly in the very early stages, and then decreases to a steady linear rate of 6.0×10^{-3} mg/cm^2/min. In the absence of wustite formation, or if wustite formation does not interfere with decarburization, then the dependence of decarburization on P_{CO_2} as predicted by Grabke[24] (equation 31) at low carbon dioxide pressures should be observed. From these data, a decarburization rate of .21 mg/cm^2/min would be expected, but the actual observed rate is much lower. The limiting tangent

of Figure 4-8 at t = 0 is about .05 mg/cm^2/min, and the rate appears to be steadily decreasing during the initial stages of oxidation to its ultimate value of .006 mg/cm^2/min. This indicates that the wustite layer decreases the oxidation rate of carbon.

At the metal surface, both iron and carbon are in competition for the adsorbed oxygen from the dissociation of CO_2 and both can react with adsorbed oxygen according to equations 15 and 30. As wustite formation progresses, sites occupied by carbon atoms become covered with wustite crystallites and the effective surface area for the carbon reaction is decreased. Then as lateral growth of the wustite proceeds, the area of metal surface exposed to the atmosphere approaches a small value. At this stage of the reaction, the atmosphere is in contact with the alloy surface only at the areas where wustite crystallites impinge upon one another. These impingement points would correspond to a large number of small pores in the scale. Comparison of the observed rate with that predicted by the Grabke analysis suggests that about 2-3% of the surface area is affected by porosity. This fraction would represent a maximum since the influence of the ratio $k_2P_{CO_2}/P_{CO}$, equation 31, has not been taken into account. The net effect is that the surface reaction for decarburization is much slower than the corresponding reaction in the absence of scale. The magnitude of decarburization for this alloy in the

CO_2 atmosphere is in close agreement with that found by Engell and Bohnenkamp[29] upon oxidizing an 0.8%C alloy in air at 950°C.

Since a constant rate of decarburization during oxidation of the alloy in CO_2 was observed irrespective of scale thickness after the surface was completely covered with scale, there are two possible explanations. Decarburization involves (1) the diffusion of carbon from the metal to the surface (2) reaction at the surface with the gas phase, and (3) transport of the reaction products through the scale. If the rate-determining step is diffusion in the metal, the carbon loss as a function of time would not be linear. Thus the rate-controlling step must be (2) the surface reaction (equation 29) or (3) transport of carbon oxides through the scale.

If the surface reaction is rate-controlling, this implies that pores in the scale are large enough to allow free passage of carbon dioxide through the scale to the surface, and also allow the carbon monoxide formed in the surface reaction to escape. If transport of CO through the scale is rate-determining, regardless of scale thickness, then it follows that there is a definite resistance to flow but it is independent of scale thickness. The resistance is not due to friction along the walls, but it may be caused by a single narrow constriction at one end, which may have been formed by lateral growth of the scale. The pores are formed at pre-existing weaknesses in the

scale, e.g., grain boundaries or dislocations, and are forced open at a critical gas pressure, corresponding to the critical content of carbon in solution. Sachs[42] has proposed this type of mechanism to account for the decarburization of Fe-C alloys in air.

5.1.3 Effect of Argon on Carbon Oxidation

In order to distinguish between the two possibilities by kinetic measurements, several experiments with argon were carried out. If the pores in the scale could be partially blocked by argon, then a decrease in decarburization rate would be expected. At P_{CO_2} = 400 mm, the oxidation rate of the alloy was observed to be .029 and .027 mg/cm^2/min with argon present, and .027 mg/cm^2/min without argon. This indicated that argon acted only as an inert diluent, and had no measurable effect on the decarburization kinetics. These results tend to support the assumption of a surface reaction being rate-determining. At P_{CO_2} = 200 mm complete coverage of the surface with wustite was not attained, and no conclusions could be drawn.

In the experiments where the gas was changed from CO_2 to argon, a slight increase in the oxidation rate of the alloy was observed. As an increase in iron oxidation rate due to argon is not feasible, this indicates a decrease in carbon oxidation rate, which may be attributed to partial blocking of the pores at a constriction as described above. On the other

hand, it may also be attributed to dilution of the gas in the pores having a greater effect on carbon oxidation than on iron oxidation. The oxidation rate of carbon was much more rapid than for iron and small changes in the partial pressure of CO_2 by argon dilution would have a larger effect on the decarburization rate. These experiments involving argon were also carried out under conditions where decarburization occured only by oxide reduction. In this case the observed rates of carbon loss were comparable to those obtained in the vacuum experiments. (Figures 4-7 and 5-1.) Since no difference was observed, it can be concluded that argon had no effect on decarburization, which means either that argon offers essentially no resistance to flow of the reacting gas through any region of the pores in a wustite scale, or that the rate of decarburization through the scale is controlled by the surface reaction (equation 29).

On the whole, the argon experiments were inconclusive in deciding whether the surface reaction or the passage of gas through the scale is the rate-determining step in decarburization through scale. The entire analysis is also complicated by the fact that decarburization by oxide reduction may be occuring simultaneously (cf. Figures 4-15 and 4-16).

5.2 Decarburization by Oxide Reduction

5.2.1 Kinetic Data

The data obtained during decarburization of a scaled specimen under vacuum according to equation 37 have been presented

in Figures 4-4 to 4-6. The results of similar experiments with argon have been shown in Figure 4-7. Wherever possible, the final points on the curves were rechecked by weighing the specimens with a microbalance, from which the average deviation of the final point was found to be about about ± 0.5 mg/cm^2. Empirical attempts were made to fit these data to linear (as previously shown), parabolic and exponential relationships, but none of these were entirely satisfactory over the whole time range. However, it may be seen that the decarburization rate is rapid during the initial stages of the reaction, and decreases continually thereafter.

In order to evaluate these data, limiting tangents at the time of changing conditions (e.g., 44 min in the complete curve presented in Figure 4-4) have been calculated. When these limiting tangents are plotted as a function of oxide thickness, which can be calculated from the observed weight change and Figure 4-8, the result is the plot shown in Figure 5-1. Although there is a considerable amount of scatter in these data, a trend may be seen towards a decrease in decarburization rate through thick scales. (The solid curve is the best straight line, as determined by the method of least-squares analysis.)

A similar trend is shown by plotting the limiting tangents as a function of carbon removed, as shown in Figure 5-2. As before, the amount of carbon removed at the time of changing conditions can be determined from Figure 4-8.

Figure 5-1 Dependence of Decarburization Rate on Oxide Thickness (calculated from limiting tangents of Figures 4-4 to 4-6).

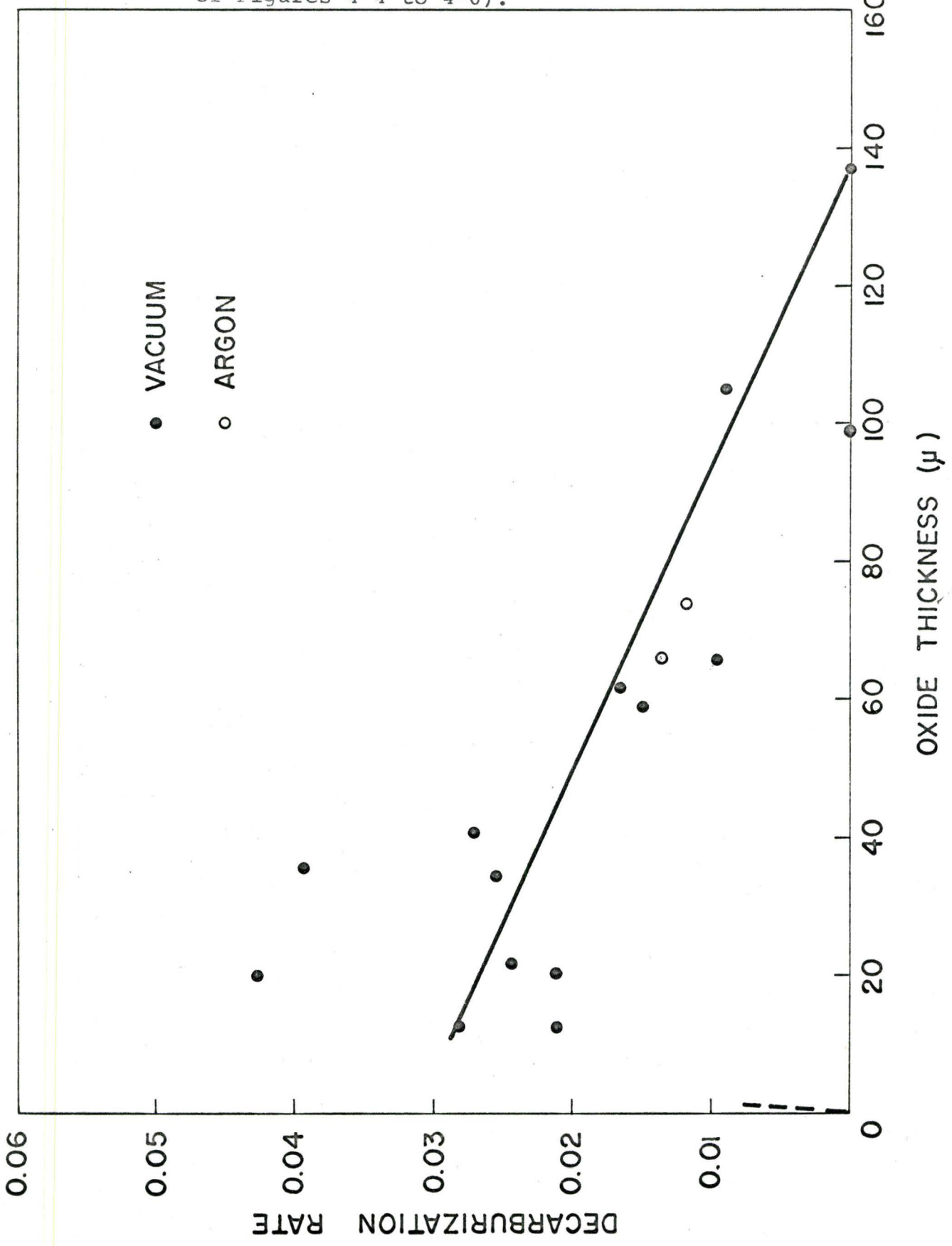

Figure 5-2 Dependence of Decarburization Rate on Carbon Removed
(Calculated from limiting tangents of Figures 4-4 to 4-6)

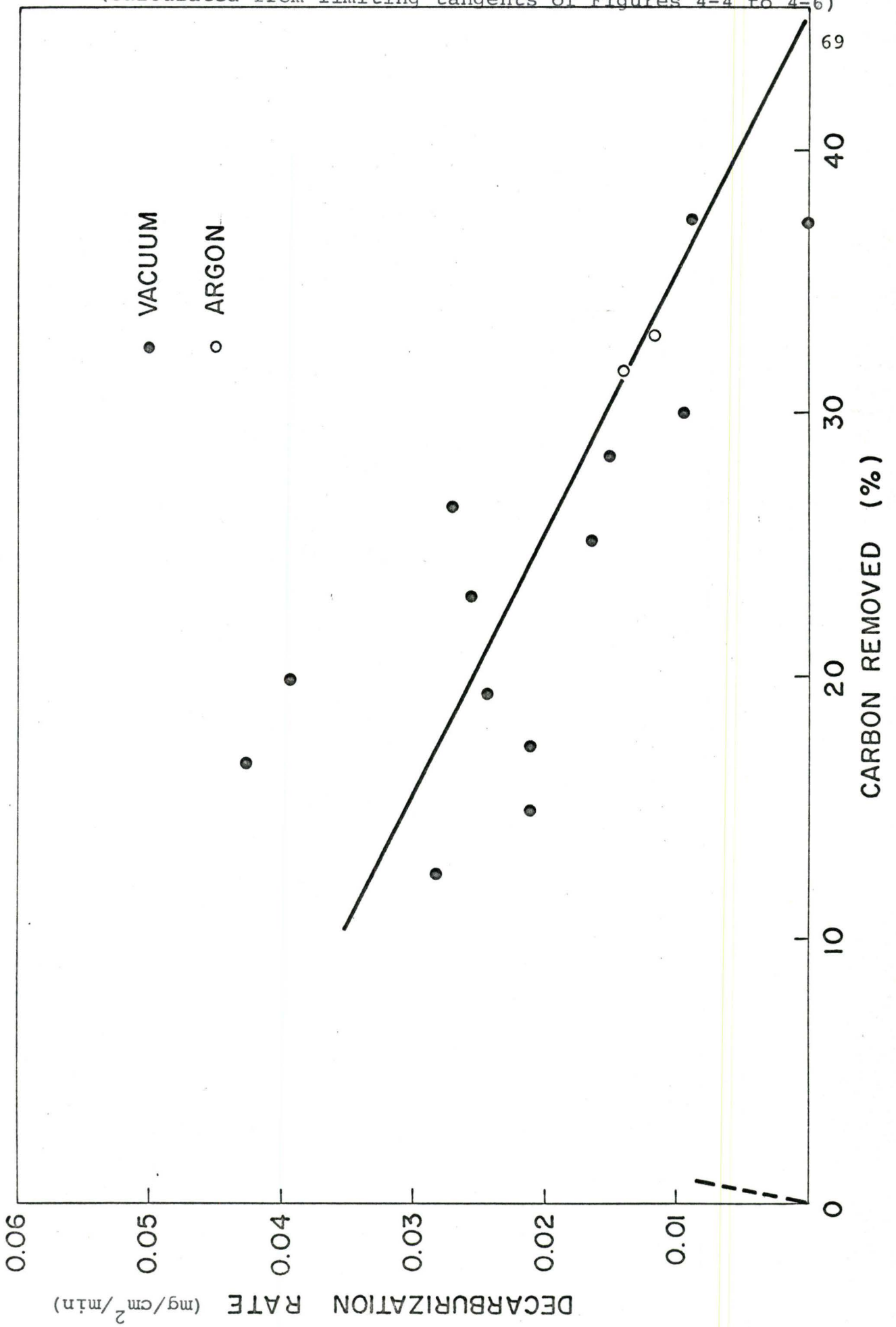

It will be noted that two of the samples showed a decarburization rate of zero. Both of these were analyzed for carbon content which was approximately 0.5%, in agreement with that predicted from the kinetic data, within the limits of experimental error. This indicates that no carbon loss occurred through these very thick scales during the time of the experiments. The data also indicate that the decarburization rate is not independent of oxide thickness, when the decarburization proceeds by oxide reduction, which is different from the case in which carbon reacts directly with the gas phase. It seems possible that in the absence of a reactive atmosphere, the reaction of carbon with the oxide (equation 37) may reach a state of equilibrium.

Direct measurements of carbon loss, by analysis of specimens with a constant oxide thickness which were decarburized under vacuum for varying times, show the same trend, i.e., the rate of decarburization decreases with time, and is slower at long times than decarburization of specimens undergoing scaling in CO_2.

5.2.2 Oxide Reduction at the Metal-Oxide Interface

Metallographic evidence indicates that reaction of carbon with the oxide occurs at the metal-oxide interface, and proceeds through the oxide layer (see Figures 4-13 and 4-17 to 4-21). The nature of the metal-oxide interface becomes very irregular, and voids are formed due to the differences in molar

volume between oxide reduced and metal formed. In one case, Figure 4-17, a graphical determination of void volume was calculated and this volume corresponded to the difference between the volume of oxide reduced and the volume of iron formed. Microscopic examination of several oxidized specimens indicated that this phenomenon was common. Other features, however, such as blistering and complete spalling of the scale from the alloy did occur. One result of the reduction is that the surface area can no longer be approximated by the geometric area, which makes evaluation of the reaction rates more difficult.

5.2.3 Equilibrium at the Metal-Oxide Interface

As mentioned above, the reaction of carbon with wustite

$$C(\gamma\text{-Fe}) + FeO \longrightarrow Fe + CO \qquad (37)$$

may reach a state of equilibrium. By applying the law of mass action, the equilibrium constant may be defined as

$$K = \frac{a_{Fe} \cdot P_{CO}}{a_{FeO} \cdot a_C} \qquad (38)$$

From equation (38), and assuming the activities of Fe and FeO to be unity, the equilibrium pressure of CO can be determined.

$$P_{CO} = K \cdot a_c \qquad (39)$$

To determine the equilibrium constant, equation (37) can be split into three partial reactions, for which thermodynamic data are available, i.e.,

$$C(\gamma\text{-Fe}) \longrightarrow C(\text{graphite}) \tag{40}$$

$$C(\text{graphite}) + \frac{1}{2}\,O_2 \longrightarrow CO \tag{41}$$

$$FeO \longrightarrow Fe + \frac{1}{2}\,O_2 \tag{42}$$

Summation of (40), (41) and (42) yields equation (37).

The free energies of equations (40), (41) and (42) respectively may be expressed as

$$\Delta F^{\circ} = -10{,}800 + 11.48T^{35} \tag{43}$$

$$\Delta F^{\circ} = -26{,}700 - 20{\cdot}95T^{36} \tag{44}$$

$$\Delta F^{\circ} = +62{,}050 - 14.95T^{36} \tag{45}$$

Summation of (43), (44) and (45) yields for the free energy of equation (37):

$$\Delta F^{\circ} = 24{,}550 - 24.42T \tag{46}$$

from which $\Delta F^{\circ}(950^{\circ}C) = -5316$ cal/mole (47)

Substituting this value in the thermodynamic relationship,

$$\log K = \frac{-\Delta F^{\circ}}{2.303RT} \tag{48}$$

a value of K for equation (37) of 8.92 is obtained. Then, substituting in equation (39), using activity data from Darken and Gurry[43], an equilibrium pressure of $P_{CO} = 2.5$ atm is obtained. Similar calculations by Engell[27] give an equilibrium pressure of 16 atm for an alloy of Fe-0.5%C at 950°C. It is emphasized that an error of ± 1000 cal in each of the free energy equations (43), (44) and (45) can change the value of the equilibrium

constant for reaction (37) by as much as a factor of six. Thus the evaluations of the carbon monoxide pressures are accurate only to a factor of ten.

It must be pointed out that there are several approximations in this method of analysis. The concentration of carbon has been taken as 0.5%, which is the average concentration of the specimens after formation of the thick resistant wustite scale. However, one cannot assume that the carbon is uniformly distributed, as microscopic examination (Figures 4-17, 4-20, 4-23 and 4-25) showed that extensive decarburization occurred near the surface, and only slight carbon depletion at the center of the specimen. Even at the surface, the carbon distribution was not uniform. Thus the calculated value represents a maximum for the equilibrium P_{CO} which would occur in the pores at the metal-oxide interface. The gas in the pores may not be entirely CO; some CO_2 may be formed.

5.2.4 Mechanical Rupture of Scale

Blistering of the scale, or in the extreme case, spalling of the scale, can occur when the pressure of carbon monoxide gas combined with the stress induced in wustite is greater than the adherence of the scale to the metal. Peters and Engell[36,37] measured the adherence of wustite to iron, iron-carbon alloys, and steels by measuring the force required to separate the scale and metal, and obtained values ranging from 100 atm. for pure iron to 30 atm. for Fe-0.6%C. Measure-

ments were made at room temperature on samples oxidized at higher temperatures, and the effect of quenching on adherence was uncertain. Nevertheless, the value of 30 atm. for the Fe-C alloy may be compared to the magnitude of 2.5 - 16 atm. calculated for the equilibrium pressure of carbon monoxide. While the former value is higher than the calculated equilibrium pressure of CO, it may not be so significantly different to make mechanical rupture of the scale impossible, when one considers the inaccuracy of the calculated equilibrium pressure and adherence measurements. In this investigation, some evidence of blister formation during oxide reduction accompanied by less depletion of carbon at the alloy surface was observed. (Figures 4-23 and 4-24.)

Oxidized specimens decarburized under vacuum generally exhibited small voids at the interface, accompanied by precipitation of iron (Figure 4-17). On some specimens, oxide spalled off at localized regions during quenching or subsequent handling, giving rise to large gaps at the metal-oxide interface. However, it is difficult to say whether these latter gaps originated during the reaction period, during quenching, or during metallographic preparation. Carbon was depleted from the alloy in these areas, indicating that blistering of the oxide from the metal was not a fundamental factor because of porosity in the wustite.

5.3 Decarburization Mechanism

The results of this investigation have demonstrated that a general feature of vacuum decarburization of oxidized specimens is the formation of voids containing metal from reduction of wustite at the metal-oxide interface. In these regions the alloy surface was depleted of carbon. It was shown in Section 4.5.2 that decarburization occurred by reaction (37) for reduction of wustite by carbon. The void volume corresponded to the difference between the volume of oxide reduced and the volume of metal formed. A carbon-depleted zone was apparent in the alloy at these regions and consequently it was not possible to determine whether the kinetics of this reaction or carbon diffusion determined the vacuum decarburization rates.

All observations were consistent with the proposal of Engell and Bohnenkamp[29] that transfer of carbon monoxide through the scale occurred by pores which remain effective only above a critical carbon content at the surface. This critical content would appear to be a complex function of the exposure atmosphere, temperature, original alloy concentration and the amount of wustite formation. The results of vacuum decarburization for the 0.8%C alloy clearly demonstrate that the pores remain effective for transfer of carbon monoxide at 950^{o}C after oxidation in carbon dioxide when the residual carbon content exceeds 0.5%. This condition applies only for vacuum decarburization in the presence of wustite and not when the specimens are exposed to an oxidizing atmosphere. Moreover,

the decarburization reaction would appear to be determined by the surface reaction for reduction of wustite and/or diffusion of carbon in the alloy since decarburization in argon had no measurable effect on the decarburization kinetics (Figure 5-1).

In this thesis, a mathematical description of the processes involving transfer of carbon monoxide through an oxide layer has not been attempted. It is possible, however, to list several points which may be relevant to such an analysis. In the range of wustite formation under oxidizing conditions, the reactions appeared to be determined by surface processes and it is essential to know the effective steady state porosity in addition to the surface reaction rate constants. At some stage of the reaction diffusion of carbon to the metal surface may be rate-determining and the pores may become ineffective for carbon monoxide transport. If these parameters were well-defined, it would be perhaps possible to carry out an analysis for the limiting cases of surface-controlled and diffusion-controlled oxidation and decarburization reactions.

CHAPTER VI

CONCLUSIONS

1. The oxidation behaviour of iron in CO_2 is practically unaffected by alloying iron with carbon.
2. Oxidation of the carbon in an iron-carbon alloy in CO_2 decreases until the metal surface is completely covered with wustite, and then continues at a constant rate for several hours at 950°C.
3. When coverage of the surface with wustite is complete, the maximum surface area affected by porosity is of the order of 2-3%.
4. The rate of carbon oxidation in a carbon dioxide atmosphere is controlled by the surface reaction of carbon with chemisorbed oxygen produced by dissociation of carbon dioxide.
5. Decarburization by oxide reduction occurs at the metal-oxide interface. The equilibrium pressure of CO thus produced is of the same order of magnitude, or less, than the pressure required for mechanical rupture. The surface formed during this process is very irregular. Void

formation at the surface corresponds to the difference in volume between oxide reduced and metal formed.

6. The most probable means of transport of carbon through the scale is porosity in the scale, although mechanical rupture of the scale is also possible.

BIBLIOGRAPHY

1. O. Kubaschewski and B. E. Hopkins, Oxidation of Metals and Alloys (1962)
2. K. Hauffe, Oxidation of Metals (1965)
3. P. Kofstad, High Temperature Oxidation of Metals (1966)
4. C. Wagner, Z. Phys. Chem. B21, 25 (1933)
5. C. Wagner and K. Ziemens, Acta. Chem. Scand., 1, 547 (1947)
6. L. Himmel, R. F. Mehl, and C. E. Bircherall, J. Metals, 5, 827 (1953)
7. N. Cabrera and N. F. Mott, Rep. Prog. Phys., 12, 163 (1949)
8. K. Hauffe and B. Ilschner,Z. Elektrochem., 58, 382 (1954)
9. L. S. Darken and R. W. Gurry, J. Am. Chem. Soc., 68, 798 (1946)
10. M. H. Davies, M. T. Simnad, and C. E. Birchenall, J. Metals, 3, 889 (1951)
11. M. H. Davies, M. T. Simnad, and C. E. Birchenell, J. Metals, 5, 1250 (1953)
12. J. Paidassi, Acta Met., 6, 184 (1958)
13. 0. Kubaschewski and D. M. Brasher, Trans. Farad. Soc., 55, 1200 (1959)
14. K. Hauffe and H. Pfeiffer, Z. Metallk., 44, 27 (1953)
15. W. W. Smeltzer, Acta Met., 8, 377 (1960)

16. E. Pettit, R. Yinger, and J. B. Wagner, Acta Met., 8, 617 (1960)

17. E. Pettit and J. B. Wagner, Acta Met., 12, 35 (1964)

18. H. J. Grabke, Ber. Bunsenges Physik. Chem., 69, 48 (1965)

19. L. A. Morris and W. W. Smeltzer, Acta Met., in press

20. R. P. Smith, J. Am. Chem. Soc., 68, 1163 (1946)

21. W. W. Webb, J. T. Norton and C. Wagner, J. Electrochem. Soc., 103, 112 (1956)

22. W. A. Pennington, Trans. A.S.M., 37, 48 (1946)

23. E. Doehlmann, Z. Elektrochem., 42, 561 (1936)

24. H. J. Grabke, Proc. 3rd Int. Cong. on Catalysis, p. 928 (1964)

25. G. J. Billings, M.Sc. Thesis, McMaster University (1966)

26. H. Eyring, J. Chem. Phys., 3, 107 (1934)

27. H. J. Engell, Z. Elektrochem., 63, 842 (1959)

28. H. J. Engell and K. Bohnenkamp, Arch. Eisen., 33, 359 (1962)

29. H. J. Engell and K. Bohnenkamp, First International Congress on Metallic Corrosion, p. 215 (1961)

30. K. Langer and H. Trenkler, Berg Huttemmann. Monatshefte, 110, 291 (1965)

31. F. K. Peters, Thesis, Technische Hochschule (1958)

32. H. Schmalzreid, private communication

33. K. Sachs and J. R. Brown, J.I.S.I., 190, 169 (1958)

34. F. D. Richardson and J. H. E. Jeffes, J.I.S.I., 160, 261 (1948)

35. F. D. Richardson, J.I.S.I., 175, 33 (1953)

36. F. K. Peters and H.J. Engell, Arch. Eisen., 28, 567 (1957)

37. F. K. Peters and H.J. Engell, Arch. Eisen., 30, 275 (1959)

38. Handbook of Chemistry and Physics, p. 3166 (1959-1960)

39. L. S. Darken and R. W. Gurry, J. Am. Chem. Soc., 67, 1398 (1945)

40. L. A. Morris, Ph.D. Thesis, McMaster University (1965)

41. G. T. F. Jay, Metallurgia, 66, 47 (1962)

42. K. Sachs, First International Congress on Metallic Corrosion, p. 219 (1961)

43. L. S. Darken and R. W. Gurry, Physical Chemistry of Metals p. 406 (1953)